Accepted Manuscript

Polymeric micelle-mediated delivery of half-sandwich ruthenium(II) complexes with phosphanes derived from fluoroloquinolones for lung adenocarcinoma treatment

Przemysław Kołoczek, Agnieszka Skórska-Stania, Agnieszka Cierniak, Victor Sebastian, Urszula K. Komarnicka, Michał Płotek, Agnieszka Kyzioł

PII: S0939-6411(18)30106-1
DOI: https://doi.org/10.1016/j.ejpb.2018.04.016
Reference: EJPB 12746

To appear in: *European Journal of Pharmaceutics and Biopharmaceutics*

Received Date: 21 January 2018
Revised Date: 5 April 2018
Accepted Date: 16 April 2018

Please cite this article as: P. Kołoczek, A. Skórska-Stania, A. Cierniak, V. Sebastian, U.K. Komarnicka, M. Płotek, A. Kyzioł, Polymeric micelle-mediated delivery of half-sandwich ruthenium(II) complexes with phosphanes derived from fluoroloquinolones for lung adenocarcinoma treatment, *European Journal of Pharmaceutics and Biopharmaceutics* (2018), doi: https://doi.org/10.1016/j.ejpb.2018.04.016

Polymeric micelle-mediated delivery of half-sandwich ruthenium(II) complexes with phosphanes derived from fluoroloquinolones for lung adenocarcinoma treatment

Przemysław Kołoczek[a], Agnieszka Skórska-Stania[a], Agnieszka Cierniak[b], Victor Sebastian[c,d], Urszula K. Komarnicka[e], Michał Płotek[a,f], Agnieszka Kyzioł[a*]

[a] *Faculty of Chemistry, Jagiellonian University in Krakow, Gronostajowa 2, 30-387 Krakow, Poland*

[b] *Department of General Biochemistry, Faculty of Biochemistry, Biophysics and Biotechnology, Jagiellonian University, Gronostajowa 7, 30-387 Kraków, Poland*

[c] *Department of Chemical Engineering, Aragon Institute of Nanoscience (INA), University of Zaragoza, Campus Río Ebro-Edificio I+D, Mariano Esquillor S/N, 50018 Zaragoza, Spain*

[d] *Networking Research Center on Bioengineering, Biomaterials and Nanomedicine, CIBER-BBN, 28-029 Madrid, Spain*

[e] *Faculty of Chemistry, University of Wroclaw, Joliot-Curie 14, 50-383 Wroclaw, Poland*

[f] *Faculty of Conservation and Restoration of Works of Art, Jan Matejko Academy of Fine Arts in Krakow, Lea 27-29, 30-052 Krakow, Poland*

Corresponding author e-mail address: kyziol@chemia.uj.edu.pl

ABSTRACT

Novel half-sandwich ruthenium(II) complexes with aminomethyl(diphenyl)phosphine derived from fluoroloquinolones (**RuPCp**, **RuPSf**, **RuPLm**, **RuPNr**) were being investigated as alternatives to well-established metal-based chemotherapeutics. All compounds were characterized by elemental analysis, selected spectroscopic methods (*i.e.*, absorption and fluorescence spectroscopy, ESI-MS, NMR, circular dichroizm), X-ray diffractometry, ICP-MS, and electrochemical techniques. To overcome low solubility, serious side effects connected with systemic cytotoxicity of ruthenium complexes, and acquiring the resistance of cancer cells, polymeric nanoformulations based on Pluronic P-123 micelles loaded with selected Ru(II) complexes were prepared and characterized. Resulting micelles (**RuPCp_M**, **RuPNr_M**) enabled efficient drug accumulation inside human lung adenocarcinoma (A549 tumor cell line), proved by confocal microscopy and ICP-MS analysis, allowing cytotoxic action. Studied complexes exhibited promising cytotoxicity *in vitro* with IC50 values significantly lower than the reference drug cisplatin. The fluorescence spectroscopic data (CT-DNA titration, cell staining *in vitro*) together with analysis of DNA fragmentation

(*pBR322* plasmid, comet assay) provided clear evidence for the interaction with DNA inducing apoptotic cell death.

Keywords: arene ruthenium(II) complexes; fluoroquinolones; polymeric micelles; drug delivery; anticancer activity

1. Introduction

Despite the medicine and pharmacology development, cancer diseases are still one of the most often causes of death in the world. Among many of organic and inorganic compounds considered as potential chemotherapeutic agents, it is supposed that the metal complexes are ones of the most promising group. Their therapeutic potential in cancer therapy has recently attracted a lot of interest mainly because metals, in particular transition metals. They exhibit unique characteristics, such as redox activity, variable coordination modes and reactivity toward the organic substrates. For instance, the chemistry of ruthenium compounds has currently received intensive scrutiny, due to increasing interest in providing new alternatives to cisplatin. Ruthenium-based complexes have been developed not only because of promising cytotoxic anticancer properties but as well due to causing fewer and less severe side effects than the corresponding platinum(II) compounds.

The discovery of therapeutic activity of (ImH)[*trans*-$RuCl_4$(DMSO)Im] (NAMI-A) and (IndH)[*trans*-$RuCl_4(Ind)_2$] (KP1019) resulted in greater interest in the field of ruthenium complexes possessing prospective cytotoxic activity, including organometallic ruthenium(II) compounds [1-5]. At present, two classes of half sandwich η^6-arene-Ru(II) complexes are of the most interest: (*i*) the monofunctional compounds, represented by [(η^6-cym)Ru(en)Cl]PF_6 (cym = 1-methyl-4-(1-methylethyl)benzene, en = 1,2-ethylenediamine) and (*ii*) the bifunctional, represented by [((η^6-cym))Ru(pta)Cl_2] (pta = 1,3,5-triaza-7-phospha-tricyclo-[3.3.1.1]decane), termed RAPTA-C. The first complex [(η^6-cym)Ru(en)Cl](PF_6) shows significant antitumor activity, comparable to that of carboplatin, towards various cancer cell lines *in vitro*. On the other hand, RAPTA-C exhibits low *in vitro* activity, while being active *in vivo*, inhibiting lung metastases in mice [6].

Furthermore, combination of two or even more multifunctional structural elements brings into play different properties of a compound and may result in improving the spectrum of biological activity, novel mechanisms of action, and modification of the pharmacokinetic

profile of the drug [7, 8]. For instance, piano-stool Ru(II) compounds containing phosphines derived from fluoroquinolones can be prominent examples of this popular strategy of combining the structural elements, adopted currently in the design of new therapeutics. Quinolones are broad-spectrum antibiotics used in human and veterinary medicine for treatment of bacterial infections. What is noteworthy, quinolones also proved to cause immunomodulation and antitumor effects by different possible mode of action *e.g.*, inhibition of the activity of HERG – one of the potassium channels, which are important proteins involved in the process of cancer cell proliferation [9]. Notably, quinolones are nowadays subject of many structural modification, including coordination compounds formation, aimed at not only defeat of increasing microbial resistance against antibiotics, but as well at potential alternatives to well-established anticancer chemotherapeutics.

In our group we are focused on synthesis and characterization of metal complexes with phosphanes – a very interesting class of ligands with great capacity to structural modifications and tuning their physicochemical and, in consequence, biological properties. The majority of ruthenium(II) aminomethylphosphanes' coordination compounds exhibited cytotoxicity *in vitro* against cancer cells close to cisplatin [10]. Moreover, the synthesized copper(I) and copper(II) complexes with phosphanes modified with quinolones (*i.e.*, ciprofloxacin **PCp**, sparfloxacin **PSf**, lomefloxacin **PLm**, norfloxacin **PNr**) turned out to be more active than the parent antibiotics, and noteworthy possessed cytotoxicity *in vitro* towards selected cancer cell lines higher than cisplatin [11-14]. These findings encouraged us to implement quinolones' phosphanes as well to half-sandwich ruthenium(II) complexes and investigate their prospective anticancer activity.

Herein, we present the synthesis, physicochemical characterization, and preliminary biological study on anticancer activity *in vitro* evaluated towards lung adenocarcinoma of four novel piano-stool ruthenium(II) complexes. These organometallic complexes are an extension of the mono(aminomethyl)phosphane complex (**RuPP$_1$**) reported recently [10], in which N-ethylpiperazine ring was replaced by heterocyclic moieties of fluoroquinolones: ciprofloxacin (**RuPCp**), sparfloxacin (**RuPSf**), norfloxacin (**RuPNr**) and lomefloxacin (**RuPLm**) (Fig.1).

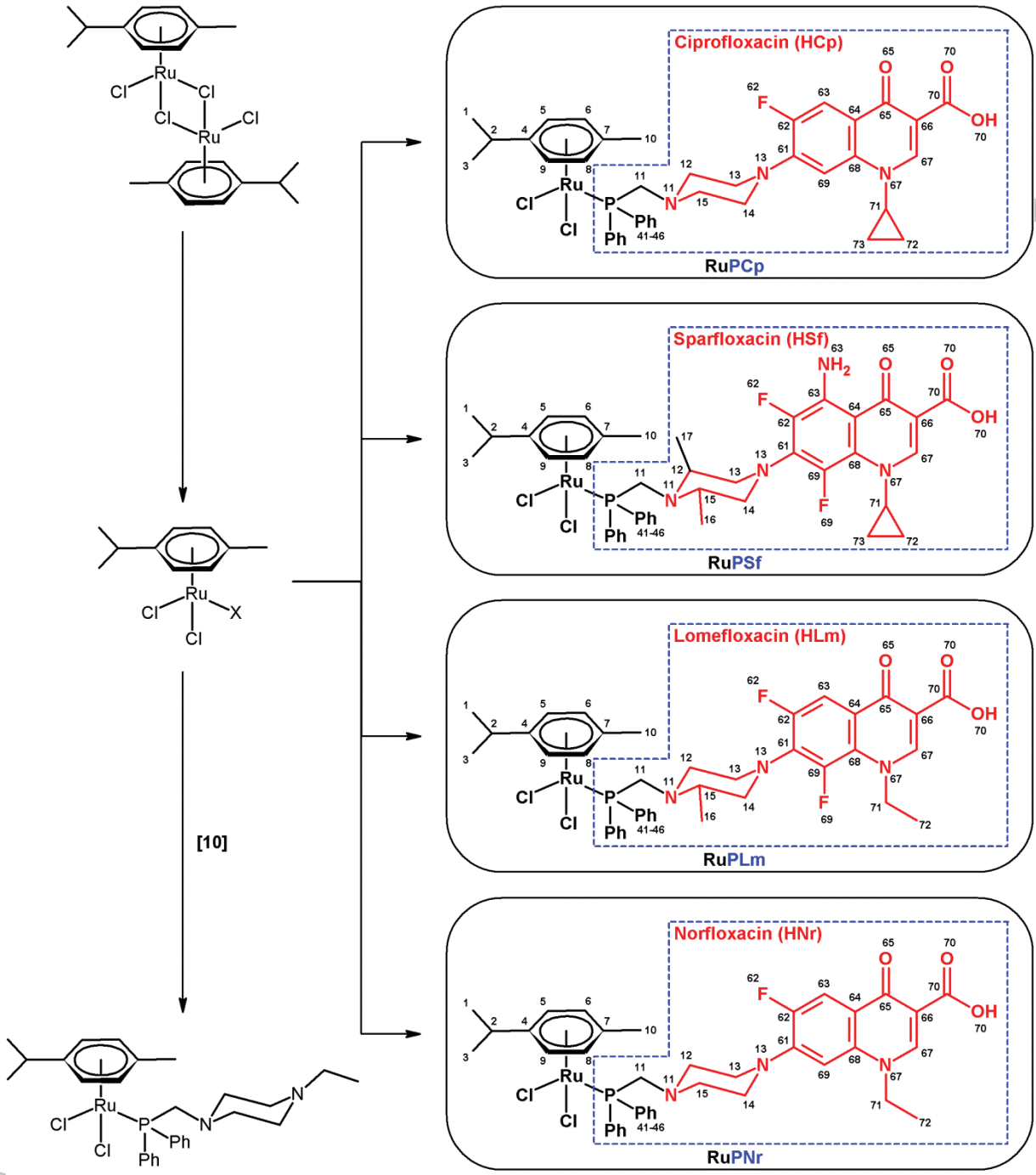

Fig. 1. Schematic view of investigated "piano-stool" ruthenium(II) compounds with phosphanes derived from fluoroquinolones.

Effective uptake of metallodrugs, for instance ruthenium complexes, by cancer cells and normal cells is important factor for selective and effective cancer therapy. The high systemic cytotoxicity of chemotherapeutics, demonstrated by the uncontrolled destruction of normal cells, as well as the development of multidrug resistance, support the need to look for

new effective targeted treatments based on nanotechnology and the changes in the molecular biology of the tumor cells. Thus, what is noteworthy, the main aim of this study was also to develop a new polymeric micellar formulation for effective ruthenium(II) complexes delivery, intended to be intravenously administered. To achieve this purpose, Pluronic P-123 (PEO_{20}-PPO_{70}-PEO_{20}) with longer hydrophobic blocks, was chosen mainly because of its commercial availability, biocompatibility and safety [15]. To the best of our knowledge, there are few reports on encapsulation of half-sandwich Ru(II) complexes into polymeric micelles [16-18]. The most advanced and innovative approach is presented by Su *et al.*, who as the first proposed self-assembled polymer-based nanocarriers for delivery of ruthenium complexes for anticancer phototherapy. Photoresponsive Ru(II)-containing block copolymers release Ru(II) complex and $^1O_2$ that both kill cancer cells [19-21].

2. Materials and methods

2.1. Reagents

All starting materials, including a 2nd (**HCp**, **HNr**, **HLm**) and 3rd (**HSf**) generation fluoroquinolones (>98%), $[Ru(\eta^6\text{-}p\text{-cymene})Cl_2]_2$ (**1**) (>98%), and Pluronic P-123 (PEO_{20}-PPO_{70}-PEO_{20}) were purchased from Sigma Aldrich and used as received. All syntheses were performed using standard Schlenk techniques. All solvents were deaerated prior to use. All obtained ruthenium complexes were dried under vacuum and increased temperature (40°C). Aminomethyl(diphenyl)phosphines: **PSf** (PPh_2CH_2**Sf**), **PCp** (PPh_2CH_2**Cp**), **PLm** (PPh_2CH_2**Lm**), and **PNr** (PPh_2CH_2**Nr**) were synthetized according to literature procedure described by our group elsewhere [22].

2.2. Structural characterization

Single crystals of **RuPCp**·$CHCl_3$·$0.5CH_3CN$, **2RuPSf**·$2CHCl_3$, **RuPLm**·$2CHCl_3$ and **RuPNr**·$2CHCl_3$ were collected on SuperNova diffractometer using graphite monochromatic MoK_α radiation at 121 K , 126 K, 119 K or 130 K, respectively. Data processing was undertaken with CrysAlisPRO [23]. The structures were solved using direct methods and for refinement the non-H atoms were treated anisotropically. The main calculations were performed with SHELXL [24] and figures were plotted with MERCURY [25]. The crystal data, experimental details and refinement results are summarized in Table S1.

Crystallographic data of the structures have been deposited at the Cambridge Crystallographic Data Centre with CCDC reference numbers CCDC 1814991 (**RuPCp**·$CHCl_3$·$0.5CH_3CN$), CCDC 1814984 (**2RuPSf**·$2CHCl_3$), CCDC 1814964 (**RuPLm**·$2CHCl_3$) and CCDC 1814944 (**RuPNr**·$2CHCl_3$).

2.3. Elemental analysis, NMR, and ESI-MS analysis

Elemental analyses (C, H and N) were carried out with Vario Micro Cube – Elementar. NMR spectra were recorded using Bruker Avance III 600 MHz and Bruker Avance II 300 MHz spectrometers in $CDCl_3$ with traces of $CHCl_3$ as an internal reference for 1H and $^{13}C\{^1H\}$, and 85% H_3PO_4 in H_2O as an external standard for $^{31}P\{^1H\}$. Mass spectra were collected with Bruker MicrOTOF-Q II spectrometer with ESI ion source in the following conditions: nebulizer pressure: 0.4 bar, dry gas: 4.0 l/min heated to 180°C. Data were recorded in the positive ion mode, while profile spectra were acquired in the mass range 50–3000 m/z; end plate offset -500V; capillary voltage 4500V; mass resolving power of the instrument - over 18,000. Mass calibration was done using the cluster method with a mixture of 10 mM sodium formate and isopropanol (1:1, v/v) before run. In order to measure spectra the compounds were dissolved in chloroform.

2.4. Synthesis and characterization of compounds

RuPCp – [Ru(η^6-*p*-cymene)Cl_2**PCp**]. Binuclear ruthenium complex **1** (0.105 g, 0.171 mmol) was added to solution of **PCp** (0.200 g, 0.378 mmol) in dichloromethane (15 ml). Resulting mixture was stirred for 24 h. After that, it was evaporated to dryness giving solid red-orange residue of product. Yield: 80%. Anal. found: C, 51.81; H, 4.67; N, 4.43%. Anal. calc. for $C_{40}H_{43}Cl_2FN_3O_3PRu\cdot CHCl_3$: C, 51.56; H, 4.64; N, 4.40%. NMR (298 K, $CDCl_3$): ^1H: 0.88 ($H^{1,3}$, d, 6.8 Hz, 6-H), 1.05-1.40 ($H^{72,73}$, m, 4-H), 1.84 (H^{10}, s, 3-H), 2.28 ($H^{13,14}$, bs, 4-H), 2.47 (H^2, spt, 6.9 Hz, 1-H), 2.92 ($H^{12,15}$, bs, 4-H), 3.46 (H^{71}, bs, 1-H), 3.89 (H^{11}, s, 2-H), 5.13 ($H^{6,8}$, d, 5.7 Hz, 2-H), 5.26 ($H^{5,9}$, d, 5.9 Hz, 2-H), 7.13 (H^{69}, d, 7.1 Hz, 1-H), 7.41-7.62 ($H^{43,44}$, m, 6-H), 7.89 (H^{63}, d, 13.3 Hz, 1-H), 7.97-8.13 (H^{42}, m, 4-H), 8.70 (H^{67}, s, 1-H), 14.99 (H^{70}, s, 1-H); $^{31}P\{^1H\}$: 27.0 (P^1, s). $^+$ESI-MS ($CHCl_3$, m/z): 1695.3 (25.0%); 1673.3 (8.73%) [2 **RuPCp**]$^+$; 1277.4 (12.4%); 858.13 (43.0%) [**RuPCp** + Na – H]$^+$; 836.15 (68.9%) [**RuPCp**]$^+$; 800.17 (17.9%) [**RuPCp** – Cl – H]$^+$; 574.16 (12.8%) [**PCp** + 2 Na]$^+$; 552.18 (100%) [**PCp** + Na]$^+$. Crystals of **RuPCp**·$CHCl_3$·1/2CH_3CN suitable for X-ray analysis were obtained at fridge by slow evaporation of acetonitrile/chloroform (1:1, v/v) solution of in normal oxygen condition. Crystal data: $C_{42}H_{44}Cl_5FN_{3.5}O_3PRu$, M = 974.1 g/mol, crystal size: 0.20 × 0.15 × 0.05 mm, crystal system: triclinic, space group: $P\bar{1}$, a = 12.2875(4) Å, b = 12.3091(4) Å, c = 14.4938(4) Å, α = 93.860(3)°, β = 90.244(3)°, γ = 105.051(3)°, V = 2111.62(12) Å^3, D_{calc} (Z = 2) = 1.532 g/cm^3, θ range for data collection: 2.995-28.550°, Mo Kα radiation (λ = 0.71073 Å), μMo = 0.774 mm^{-1}, reflections collected/unique: 30334/9763, [R_{int} = 0.0340], completeness to θ full = 99.5%, final R indices [I > 2σ(I)]: R_1 = 0.0376, wR_2

= 0.0912, R indices (all data): R_1 = 0.0508, wR_2 = 0.1002, GOF = 1.049, largest diff. peak and hole: 1.134 and -1.038 eÅ^{-3} , data/restraints/parameters: 9763/0/519, T = 121 K.

RuPSf – [Ru(η^6-*p*-cymene)Cl_2**PSf**]. Following the method presented for **RuPCp**, **1** (0.094 g, 0.153 mmol) and **PSf** (0.200 g, 0.339 mmol) gave red-orange precipitate. Yield: 80%. Anal. found: C, 50.57; H, 4.73; N, 5.51%. Anal. calc. for $C_{42}H_{47}Cl_2F_2N_4O_3PRu{\cdot}CHCl_3$: C, 50.82; H, 4.76; N, 5.51%. NMR (298 K, $CDCl_3$): ^{1}H: 0.89 ($H^{16, 17}$, d, 6.7 Hz, 6-H), 0.96 ($H^{1, 3}$, d, 7.0 Hz, 6-H), 1.02-1.27 ($H^{72, 73}$, m, 4-H), 1.78 (H^{10}, s, 3-H), 2.29 ($H^{12, 15}$, m, 2-H), 2.48 (H^2, spt, 7.0 Hz, 1-H), 2.76 ($H^{13, 14}$, d, 10.9 Hz, 2-H), 2.95 ($H^{13, 14}$, d, 11.2 Hz, 2-H), 3.85 (H^{71}, m, 1-H), 4.05 (H^{11}, d, 2.9 Hz, 2-H), 5.15 ($H^{5, 6, 8, 9}$, m, 4-H), 6.39 (H^{63}, bs, 2-H), 7.40-7.60 ($H^{43, 44}$, m, 6-H), 7.98-8.17 (H^{42}, m, 4-H), 8.60 (H^{67}, s, 1-H), 14.61 (H^{70}, s, 1-H); ^{31}P{^{1}H}: 25.7 (P^1, s). $^+$ESI-MS ($CHCl_3$, m/z): 1104.8 (10.8%); 919.17 (12.0%) [**RuPSf** + Na]$^+$; 897.18 (19.1%) [**RuPSf** + H]$^+$; 855.25 (33.5%) [**RuPSf** – cyclopropane]$^+$; 824.74 (22.4%); 393.18 (100%) [**Sf** + H]$^+$. Crystals of 2**RuPSf**·2$CHCl_3$ suitable for X-ray analysis were obtained at fridge by slow diffusion of diethyl ether to solution of the complex in chloroform in normal oxygen condition. Crystal data: $C_{86}H_{96}Cl_{10}F_4N_8O_6P_2Ru_2$, M = 2032.3 g/mol, crystal size: 0.20 × 0.10 × 0.03 mm, crystal system: triclinic, space group: $P\bar{1}$, a = 13.7041(3) Å, b = 16.8129(6) Å, c = 20.9633(6) Å, α = 71.016(3)°, β = 75.581(2)°, γ = 78.123(3)°, V = 4382.2(2) Å^3, D_{calc} (Z = 2) = 1.540 g/cm^3, θ range for data collection: 2.841-28.601°, Mo Kα radiation (λ = 0.71073 Å), μMo = 0.752 mm^{-1}, reflections collected/unique: 66135/20347, [R_{int} = 0.0724], completeness to θ full = 99.8%, final R indices [I > 2σ(I)]: R_1 = 0.0628, wR_2 = 0.1429, R indices (all data): R_1 = 0.1129, wR_2 = 0.1759, GOF = 1.035, largest diff. peak and hole: 1.847 and -1.431 eÅ^{-3} , data/restraints/parameters: 20347/0/1087, T = 126 K.

RuPLm – [Ru(η^6-*p*-cymene)Cl_2**PLm**]. Following the method presented for **RuPCp**, **1** (0.101 g, 0.165 mmol) and **PLm** (0.200 g, 0.364 mmol) gave red-orange precipitate. Yield: 80%. Anal. found: C, 56.27; H, 5.19; N, 4.88%. Anal. calc. for $C_{40}H_{44}Cl_2F_2N_3O_3PRu$: C, 56.14; H, 5.18; N, 4.91%. NMR (298 K, $CDCl_3$): ^{1}H: 0.67 (H^{16}, d, 6.3 Hz, 3-H), 0.91 ($H^{1, 3}$, d, 6.9 Hz, 3-H), 0.99 ($H^{1, 3}$, d, 6.9 Hz, 3-H), 1.49 (H^{72}, t, 6.8 Hz, 3-H), 1.79 (H^{10}, s, 3-H), 1.98-3.10 ($H^{12, 13, 14, 15}$, m, 7-H), 2.47 (H^2, spt, 7.0 Hz, 1-H), 3.84-4.04 (H^{11}, m, 2-H), 4.39 (H^{71}, qd, J_1 = 6.9 Hz, J_2 = 3.3 Hz, 2-H), 5.03-5.28 ($H^{5, 6, 8, 9}$, m, 4-H), 7.40-7.60 ($H^{43, 44}$, m, 6-H), 7.85 (H^{63}, dd, J_1 = 12.0 Hz, J_2 = 1.9 Hz, 1-H), 7.96-8.14 (H^{42}, m, 4-H), 8.54 (H^{67}, s, 1-H), 14.67 (H^{70}, s, 1-H); ^{31}P{^{1}H}: 26.1 (P^1, s). $^+$ESI-MS ($CHCl_3$, m/z): 878.14 (30.0%) [**RuPLm** + Na]$^+$; 856.16 (100%) [**RuPLm** + H]$^+$; 820.18 (84.8%) [**RuPLm** – Cl]$^+$; 784.21 (9.64%) [2 (**RuPLm** – Cl – H)]$^{2+}$; 572.19 (42.5%) [**PLm** + Na]$^+$; 364.16 (15.2%) [CH_2-**Lm**]$^+$; 352.15 (9.78%) [**Lm**

+ H]$^+$; 328.94 (13.3%); 301.14 (22.3%). Crystals of **RuPLm**·2CHCl$_3$ suitable for X-ray analysis were obtained at fridge by slow evaporation of chloroform/toluene (1:3, v/v) solution of in normal oxygen condition. Crystal data: $C_{42}H_{46}Cl_8F_2N_3O_3PRu$, M = 1094.5 g/mol, crystal size: 0.39 × 0.13 × 0.12 mm, crystal system: monoclinic, space group: $P2_1/n$, a = 29.2597(6) Å, b = 16.9010(3) Å, c = 9.8988(2) Å, α = 90°, β = 109.865(2)°, γ = 90°, V = 4603.85(17) Å^3, D_{calc} (Z = 4) = 1.578 g/cm^3, θ range for data collection: 2.961-28.699°, Mo Kα radiation (λ = 0.71073 Å), μMo = 0.890 mm^{-1}, reflections collected/unique: 65161/11131, [R_{int} = 0.0690], completeness to θ full = 99.7%, final R indices [I > 2σ(I)]: R_1 = 0.0749, wR_2 = 0.1677, R indices (all data): R_1 = 0.0959, wR_2 = 0.1762, GOF = 1.188, largest diff. peak and hole: 1.160 and -0.707 eÅ^{-3} , data/restraints/parameters: 11131/0/558, T = 119 K.

RuPNr – [Ru(η^6-*p*-cymene)Cl$_2$**PNr**]. Following the method presented for **RuPCp**, **1** (0.108 g, 0.176 mmol) and **PNr** (0.200 g, 0.386 mmol) gave red-orange precipitate. Yield: 80%. Anal. found: C, 56.99; H, 5.24; N, 5.07%. Anal. calc. for $C_{39}H_{43}Cl_2FN_3O_3PRu$: C, 56.87; H, 5.26; N, 5.10%. NMR (298 K, $CDCl_3$): ^{1}H: 0.89 ($H^{1,3}$, d, 6.9 Hz, 6-H), 1.53 (H^{72}, t, 6.8 Hz, 3-H), 1.85 (H^{10}, s, 3-H), 2.29 ($H^{13,14}$, bt, 4-H), 2.48 (H^2, spt, 7.0 Hz, 1-H), 2.90 ($H^{12,15}$, bt, 4-H), 3.89 (H^{11}, s, 2-H), 4.23 (H^{71}, q, 7.1 Hz, 2-H), 5.14 ($H^{6,8}$, d, 6.1 Hz, 2-H), 5.26 ($H^{5,9}$, d, 5.9 Hz, 2-H), 6.61 (H^{69}, d, 7.0 Hz, 1-H), 7.44-7.60 ($H^{43,44}$, m, 6-H), 7.97 (H^{63}, d, 13.3 Hz, 1-H), 8.00-8.15 (H^{42}, m, 4-H), 8.62 (H^{67}, s, 1-H), 15.07 (H^{70}, s, 1-H); ^{31}P{^{1}H}: 26.9 (P^1, s). $^+$ESI-MS ($CHCl_3$, m/z): 1058.16 (45.3%); 952.14 (19.1%); 923.17 (40.2%); 824.15 (15.4%) [**RuPNr** + H]$^+$; 788.18 (78.3%) [**RuPNr** – Cl]$^+$; 752.20 (20.6%) [**RuPNr** – 2 Cl – H]$^+$; 564.09 (23.9%); 540.08 (45.4%); 511.60 (100%); 328.94 (22.1%); 255.58 (16.6%). Crystals of **RuPCp**·2CHCl$_3$ suitable for X-ray analysis were obtained at fridge by slow diffusion of hexane to solution of the complex in chloroform in normal oxygen condition. Crystal data: $C_{41}H_{45}Cl_8FN_3O_3PRu$, M = 1062.4 g/mol, crystal size: 0.30 × 0.05 × 0.05 mm, crystal system: triclinic, space group: $P\bar{1}$, a = 11.2574(2) Å, b = 14.6608(7) Å, c = 15.7165(6) Å, α = 116.613(4)°, β = 95.054(2)°, γ = 95.231(3)°, V = 2285.07(16) Å^3, D_{calc} (Z = 2) = 1.544 g/cm^3, θ range for data collection: 2.930-28.522°, Mo Kα radiation (λ = 0.71073 Å), μMo = 0.891 mm^{-1}, reflections collected/unique: 30595/10379, [R_{int} = 0.0485], completeness to θ full = 99.3%, final R indices [I > 2σ(I)]: R_1 = 0.0671, wR_2 = 0.1809, R indices (all data): R_1 = 0.0886, wR_2 = 0.2006, GOF = 1.047, largest diff. peak and hole: 3.013 and -1.694 eÅ^{-3} , data/restraints/parameters: 10379/0/537, T = 130 K.

2.5. Electrochemical characterization

Cyclic voltammetry (CV) for 1 mM ruthenium(II) complexes was carried out on an electrochemical analyser (Bio-Logic, SP-150). Three-electrode glass cell with a working electrode – graphite disk electrode (2 mm diameter), a counter electrode – Pt wire, and a pseudo-reference electrode – Ag wire (Ag/Ag^+, 0.01M $AgNO_3$, 0.1M tetrabutyl ammonium perchlorate (Bu_4NClO_4). All measurements were done in dimethylformamide (DMF) with 0.05M Bu_4NClO_4 as a supporting electrolyte at room temperature with scan rate 10 mV s^{-1} in the potential range from -0.5 to 1.2V *vs* Ag/Ag^+. Scans start at 0V *vs* Ag/Ag^+ in the positive potential direction. All reported potentials were converted *vs* the ferrocene/ferrocenium redox couple ($Fc^{0/+}$) [26].

2.6. Interactions with CT-DNA

The stock solution of calf thymus DNA (CT-DNA) was prepared in 50 mM PBS (pH = 7.4). The concentration of CT-DNA was determined by spectrophotometer using molar absorption coefficient 6600 M^{-1} cm^{-1} at 260 nm. Stock solution was stored in a fridge and used for no longer than 4 days. Complex of CT-DNA and ethidium bromide (EB) was prepared by mixing the substrates in equimolar ratio ($5 \cdot 10^{-5}$ M) with PBS. Fluorescence emission was recorded on spectrofluorimeter (Perkin Elmer LS55) at excitation wavelength equal to 510 nm, both emission and excitation slits widths were set to 5.0 nm. Kinetic assay was performed by fluorescence quenching of CT-DNA-EB complex by ruthenium compounds in 10-fold molar excess (*i.e.* molar ratio CT-DNA:EB:Ru was equal to 1:1:10). Appropriate aliquot of ruthenium complex solution in $CHCl_3$ in fluorescence cuvette was evaporated. Then, 3 ml of CT-DNA-EB mixture was added to obtained thin-film of ruthenium compound and fluorescence was measured immediately. Stern-Volmer plots were obtained by titration CT-DNA-EB system with Ru complexes in molar ratios 1:1:1, 1:1:2, 1:1:5, 1:1:10 and 1:1:20 (CT-DNA:EB:Ru) after 30 min incubation time. The emission and excitation slits widths were set to 5.0 nm.

2.7. DNA strand break analysis

In order to check the ability of **RuPCp**, **RuPSf**, **RuPLm** and **RuPNr** to induce single- or double-strand breaks in DNA the gel electrophoresis with *pBR322* plasmid was performed. Compounds concentrations were equal to 100, 80, 60 and 40 μM in DMF. After 1h incubation time at 37°C, 20 μl reaction mixtures were mixed with 3 μl loading buffer (bromophenol blue in 30% glycerol) and loaded on 2% agarose gels (with EB) in TBE buffer (90 mM TRIS-borate, 20 mM EDTA, pH = 8.0). Electrophoresis was conducted at constant voltage (115 V),

for 3h. At the end gel was photographed and processed with Digital Imaging System (GelDocIt).

2.8. Preparation of micelles

In the round-bottom flask 0.25 g of Pluronic P-123 was dissolved in $CHCl_3$ in 60°C, under reflux for 15 min. 1 ml of 0.5 mg/ml ruthenium compound and 1 ml of $CHCl_3$ were added to hot solution and refluxed for 15 min. Solvent was slowly evaporated on rotary evaporator in 50°C and 500 mbar with speed rotation 270 rpm. Then, obtained thin film was dried under pressure reduced to 15 mbar for 15 min. Flask was transferred to sonication bath and 20 aliquots of 0.5 ml of PBS were added to film. Obtained solution was sonicated further for 15 min 0.1 ml of resulting solution was transferred to 0.9 ml of PBS in order to determine the size of the micelles. The rest of solution was centrifuged (5000 rpm, 15 min) and obtained residue was lyophilized. The supernatant was used to check the concentration of non-encapsulated ruthenium complex utilizing ICP-MS technique (Perkin Elmer ELAN 6100). Drug loading content (LC) and encapsulation efficiency (EE) were calculated using equations:

$$LC = \frac{m_0 - m_1}{m_t} \cdot 100\%$$

$$EE = \frac{m_0 - m_1}{m_0} \cdot 100\%$$

where:

m_0 – the starting mass of ruthenium complex before synthesis [g],

m_1 – the mass of ruthenium complex in supernatant after synthesis [g],

m_t – the total mass of micelles [g].

Micelles morphology was investigated with application of transmission electron microscopy (FEI^{TM} Tecnai G2 T20). Micelles were dropped in a carbon coated copper grid, dried at room temperature and stained with a negative staining agent (phosphotungstic acid). The size distribution was determined from the enlarged TEM micrographs, using ImageJ software, counting at least 200 particles in different images. The size were also examined by dynamic light scattering techniques (DLS, ZetaSizer Nano ZS, Malvern Instruments).

2.9. Cell line

A549 cell line (human lung adenocarcinoma, morphology: epithelial, ATCC: CCL-185) was cultured in Dulbecco's Modified Eagle's Medium (DMEM, Corning) with phenol red, supplemented with 10% fetal bovine serum (FBS) and with 1% streptomycin/penicillin. Cells were cultured at 37°C under a humidified atmosphere containing 5% CO_2. Passages were

carried out using a solution containing 0.05% trypsin and 0.5 mM EDTA. All experiments were performed on cells in the logarithmic phase of growth.

2.10. Cytotoxic assay

MTT (3-(4,5-dimethylthiazol-2-yl)-2,5-diphenyltetrazolium bromide) assay was performed according the protocols described elsewhere [27]. In brief, 1×10^4 cells per well were seeded in 96-well flat bottom microtiter plate and were incubated with the tested Pluronic P-123 micelles loaded with **RuPCp** or **RuPNr** complexes (**RuPCp_M** and **RuPNr_M**, respectively) at various range of concentrations (0.2-20 μM) for 24 hours. After this, supernatants were pipetted out carefully and each well was washed with PBS. A further 24 hours was allowed for the cells to recover in drug-free medium. Afterwards, cell viability was examined and IC50 was calculated using the Hill equation (Origin 9.0) with regard to the untreated cells (control). Each compound concentration was tested in five replicates and repeated at least three times. Determined values of IC50 are given as mean + S.D. (Standard Deviation). As well, cells after treatment were intravital stained with two commercially available dyes – acridine orange (AO, 5 mg/mL) and propidium iodide (PI, 5 mg/mL). Cells were incubated with dyes for 20 min in standard conditions, then dyes were removed, cells were washed with PBS twice, and examined using a fluorescence inverted microscope (Olympus IC51, Japan) with an excitation filter 470/20 nm.

2.11. Cellular uptake

A549 cells at density of 2×10^6 cells/2 mL were seeded on 6-well plates and were incubated with **RuPCp_M** and **RuPNr_M** formulations (2 μM) for 4 or 24h at standard conditions (37°C, 5% CO_2). Additional plates were incubated with medium alone as negative control. Then, compound solutions were removed, the cells were washed twice with PBS buffer and trypsinized. The number of cells in each sample was counted manually and cells were centrifuged to obtain the whole cell pellet for analysis. For ICP-MS (inductively coupled plasma mass spectrometry) analysis cells were mineralized in 1 mL of 65% HNO_3 at 60ºC for 1 hour. Measurement of the concentration of ruthenium ions was carried out using a mass spectrometer (ELAN 6100 Perkin Elmer) with an inductively coupled plasma (ICP-MS). The copper content under each condition is expressed as μg/ml Ru per 10^6 cells. The experiment was repeated at least 3 times and results are presented as mean value + S.D..

2.12. Confocal microscopy

Confocal laser scanning microscopy (CLSM Nikon) was applied to visualize the intracellular accumulation of selected Pluronic P-123 Ru(II) complex formulation

(**RuPCp_M**). In brief, A549 cells at a density of 5×10^5 cells/mL were seeded on coverslips in 9-well plates and incubated for 24h allowing proper adhesion. Then, the growth medium was replaced with a medium containing 2 μM **RuPCp_M** and incubated for 4h at 37ºC in a humidified atmosphere containing 5% CO_2. After this time, the cells were washed twice with PBS buffer and fixed by treating firstly with 2.5% glutaraldehyde in PBS and secondly with an increasing concentration gradient of ethanol (20, 40, 60, 80 and 99%). Samples were directly imaged under a Nikon A1 confocal laser scanning system (CM) attached to an inverted microscope Nikon Ti (Japan). A 1009 objective lens (Nikon Plan Apo VC/1.40 oil) was used. The samples were excited with diode lasers (405 and 488 nm). Fluorescence spectra were collected using a 32-channel spectral detector.

2.13. Comet assay

The level of DNA damage was determined by the electrophoresis of single cells in agarose gel as earlier described [13]. Briefly, the cell suspension was mixed with low melting point agarose, set on slides, lysed and neutralized in appropriate buffers. Electrophoresis was performed at 23V (0.74 V/cm, 300 mA) for 30 min at 4°C. All stages of the experiment were carried out in the dark to eliminate any extra DNA damages. Prior to analysis the slides were stained with propidium iodide (2.5 μg/ml). The analysis of DNA damage was carried out with COMET PLUS 2.9 software (Comet Plus, Theta System GmbH, Germany). The percentage content of DNA in the comet's tail (%DNA) was determined from 100 random images of comets per slide. The analysis was done in three replicates.

3. Results and discussion

3.1. Structural characterization

The products of syntheses were recrystallized in order to obtain pure complexes. Their purity were confirmed using elemental analysis, while the single crystals were analysed by X-ray diffraction technique (Fig. 2, SI, Table S1).

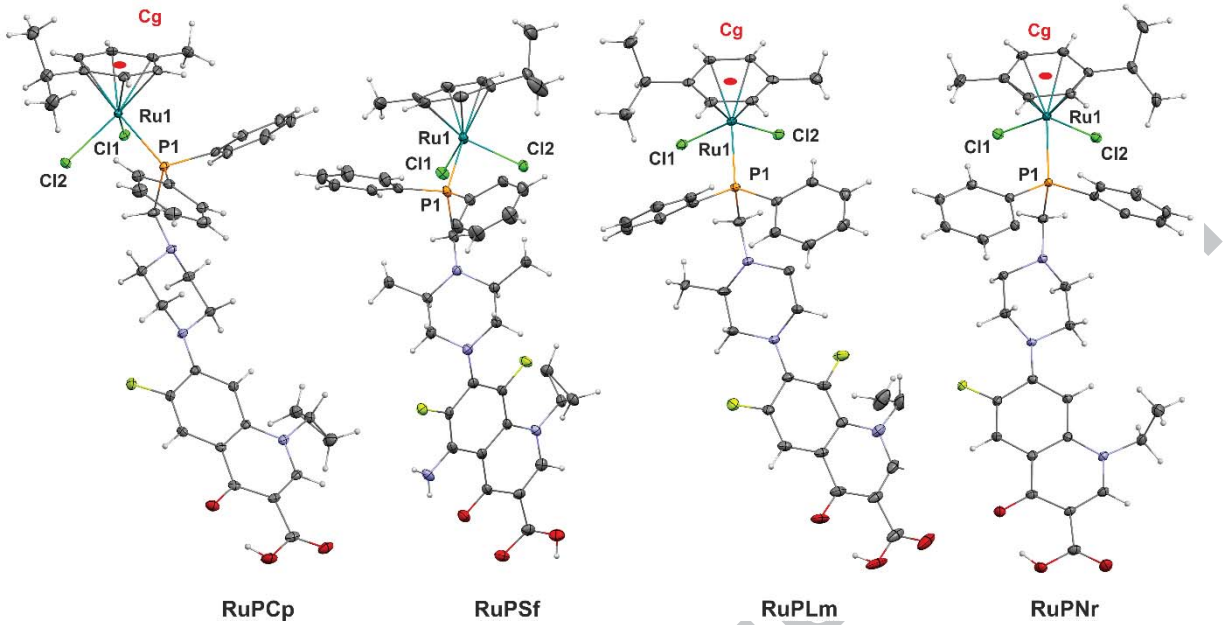

Fig. 2. Crystal structures of the complex molecules **RuPCp**, **RuPNr**, **RuPLm**, and **RuPSf** (30% probability ellipsoids). The solvents' molecules and some hydrogen atoms were omitted for clarity.

All obtained ruthenium complexes crystallized in $P\bar{1}$ space group with one exception – **RuPLm**·2$CHCl_3$, which crystalized in $P2_1/c$ space group. What is noteworthy, in the case of **2RuPSf**·2$CHCl_3$, both molecules of **RuPSf** in asymmetry unit adopt slightly different conformation (SI, Fig. S1), whereas, in the case of the other three complexes, there is only one molecule in the asymmetric unit. Coordination of phosphanes derived from fluoroquionolones did not cause significant changes in the ruthenium surrounding. Namely, only a slight increment in distance between Ru^{2+} ion and center of gravity of *p*-cymene ring (C_g) is observed (from 1.647 Å in parent dinuclear ruthenium(II) complex – **1** [10, 28], to about 1.707 Å - average distance for all complexes). Moreover, the length of Ru-Cl bonds decreased insignificantly from 2.444 Å to 2.416 Å (average for all complexes). The angle Cl-Ru-C_g is higher in complexes comparing to dimeric ruthenium substrate of 2.7°. Mentioned changes in ruthenium(II) ion surrounding are very close to observed in time of **RuPP$_1$** formation [10]. This suggests that extension of piperazine ring with heterocyclic moiety of fluoroquionolones do not affect the Ru-phosphane coordination significantly.

The $^{31}P\{^1H\}$ NMR analysis, very useful method for preliminary determination of sample purity, was applied to verify if the product of synthesis is desired one (SI, Table S2). First of all, the signal of uncoordinated aminomethylphosphane is situated in the negative part of

spectrum (**PCp**: –27.4 ppm; **PSf**: –35.9 ppm; **PLm**: –27.4 ppm; **PNr**: –27.5 ppm) and undergoes a downfield shift to the positive part of spectrum as a result of phosphane coordination (**RuPCp**: 27.0 ppm; **RuPSf**: 25.7 ppm; **RuPLm** 26.1 ppm; **RuPNr**: 26.9 ppm). Absence of other signals in spectrum confirms that coordination compound is the only one product of synthesis, free from phosphane derivatives (*e.g.*, phosphane oxides). Secondly, ^{1}H NMR measurement evidenced that phosphane coordination does not affect significantly density of electron in fluoroquinolone part. The heterocycle protons' signals are shifted less than 0.21 ppm comparing to uncoordinated phosphane. Formation of bond between ruthenium and fluoroquinolone phosphane induces the changes in ^{1}H NMR spectrum of cymene close to these observed in time of $RuPP_1$ formation. Namely, H^1-H^{10} undergoes upfield shift independently of the type of substituent bonded to piperazine ring. The isopropyl H^1 and H^3 protons are equivalent and observed as doublet in spectra of **RuPCp**, **RuPSf** and **RuPNr**, but interestingly not in the case of **RuPLm**. In spectrum of this complex the methyl groups appear as two separated doublets. This suggests that rotation of isopropyl group in **RuPLm** is inhibited.

Furthermore, mass spectrometry results confirmed the structures of prepared coordination compounds. The complexes were ionized within chloride detaching, H^+ or Na^+ connection or ruthenium oxidation. Generally, **RuPCp**, **RuPSf**, **RuPLm** and **RuPNr** turned out to be susceptible to fragmentation in measurement condition, therefore plenty of signals were observed in complexes' spectra, what made obtained spectra difficult for unambiguously interpretation (SI, Fig. S2-S5).

It is well-documented in literature, that replacement of the chloride by a DNA fragment in the coordination sphere of the metal results in formation a covalent bonds between them, what accounts for the cytotoxicity of organoruthenium species [29-31]. In the case of complexes with the general formula [(η^6-arene)Ru(L)Cl_2] (L = ligand) aquation seems to be important step in cytotoxicity, producing the ruthenium active site in order to react with biomacromolecules *i.e.*, proteins, DNA. The **RuPCp**, **RuPSf**, **RuPLm**, and **RuPNr**, similar to previously published **$RuPP_1$**, in controlled condition are hydrolysed very slowly [10]. Nevertheless, in cellular environment there is a plethora of electron-donating species and in such conditions the substitution of any ligand cannot be excluded. Furthermore, it is well-known that hydrolysis, that is suppressed extracellularly, due to the high chloride concentration (104 mM), it occurs inside the cell, in cytoplasm or the nucleus, where the chloride concentration is significantly lower [6]. Thus, presumably, the studied complexes

will hydrolyze relatively very slowly inside tumor cells, reaching the equilibrium with an amount of the complex remaining non-hydrolyzed. Indeed, both hydrolyzed and non-hydrolyzed complexes are able to interact with DNA (directly or through its ligands, respectively), thereby causing significant alterations to DNA structure. Importantly, also the non-hydrolyzed forms of **RuPCp**, **RuPSf**, **RuPLm** and **RuPNr** are able to interact with DNA (through fluoroquinolones or arene), therefore presumably the hydrolysis may not be the crucial process in case of synthesized complexes.

3.2. Electrochemical characterization

The reactivity of metal-based drugs depends largely on their ligand environment and coordination geometry, which is also determined the redox properties. The knowledge of metal-centered redox potentials can provide an essential information for the design of new complexes and a better understanding of the role of metallodrugs in biological applications. The electrochemical properties of ruthenium(II) complexes were investigated in order to assess and understand their potential role in cellular signaling through redox chemistry. Any disturbances of intracellular redox processes may significantly influences on a plethora of cellular processes such as right proliferation. This may, in turn, result in serious consequences including cell death [32].

The redox properties of new Ru(II) complexes and the corresponding ligands alone were determined by cyclic voltammetry in dimethylformamide (DMF) solutions (1 mM) using 0.1 M tetrabutyl ammonium perchlorate (TBAP) as the supporting electrolyte in the selected potential window from -0.5 V to 1.2 V *vs* Ag/Ag^{+} at a scan rate of 10 mV/s. The cyclic voltammetric responses obtained for all studied complexes with apparent oxidation peaks localized at *ca.* 0.6 V and 0.9 V *vs* $Fc^{0/+}$ are presented in Fig. 3.

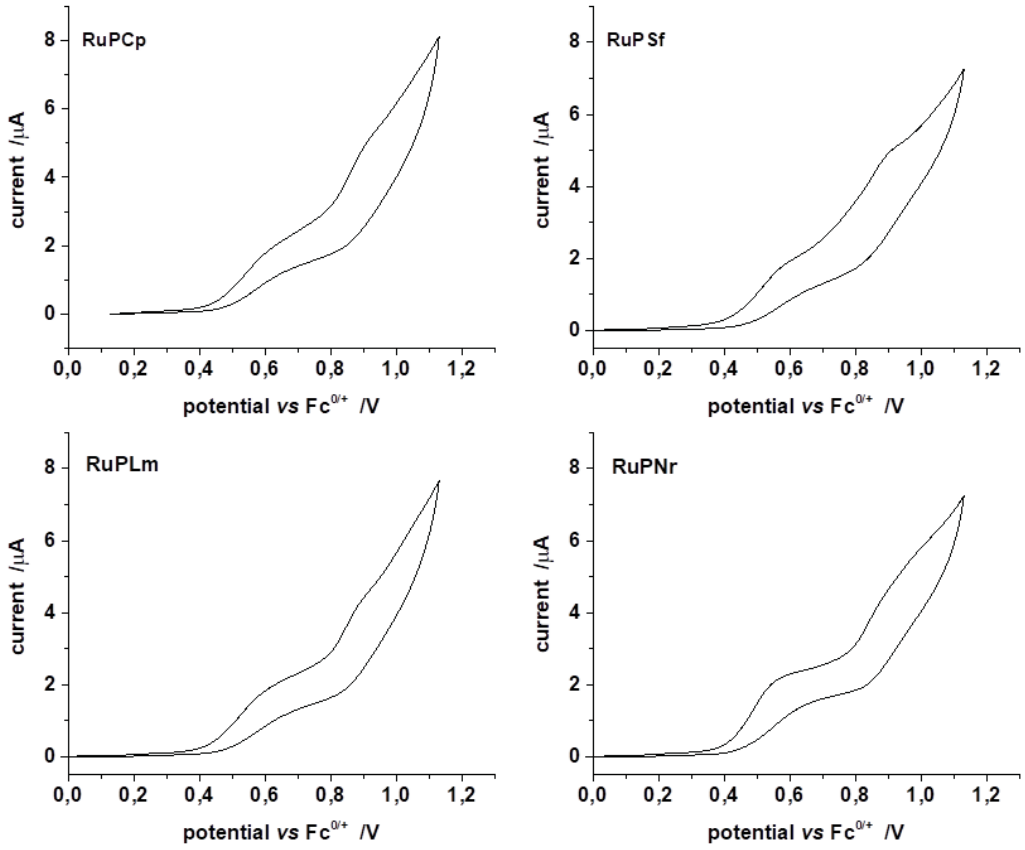

Fig. 3. Cyclic voltammograms of **RuPCp**, **RuPSpf**, **RuPLm**, and **RuPNr** ruthenium(II) complexes in DMF (1 mM). Scan rate: 10 mV/s. The potentials were referenced to the $Fc^{0/+}$ redox couple.

All the complexes displayed irreversible one-electron redox waves which can be attributed to Ru(II) ion oxidation at *ca.* 0.6 V *vs* $Fc^{0/+}$. The determined oxidation potentials for studied ruthenium(II) complexes, referring to Ru(II)/(III) redox process, are in agreement with literature data for other organometallic Ru(II) compounds [30, 33, 34]. Additional peaks, observed in cyclic voltammograms of studied complexes, can be safely associated with oxidation processes within ligand moiety on comparing with the electrochemical data of ligands alone (SI, Fig. S7). From the electrochemical data, it can be concluded that the present ligand systems in form of aminomethylophoshine derivatives of antibiotics do not stabilize the oxidation state of ruthenium(II) ion. This means, that the investigated complexes are not electrochemically stable, suggested by observed some instability of the oxidized ruthenium species at the electrode surface. However, it can be presumed that the electron transfer reactions take place without gross changes in the stereochemistry of the

complexes, that can be monitored by UV-vis spectroscopy. In UV-vis spectra no significant changes were observed, indicating the formation of completely new chemical compounds, as only decrease in absorption were detected after electrochemical study (SI, Fig. S8). What is also noteworthy, monitored changes in UV-vis spectra during 24 hours in DMF solvent did not revealed spectral changes implicating ligands exchange due to DMF coordination (SI, Fig. S9). Thus, even though it is stated that Ru(II) arene "piano-stool" complexes are normally unable to change their +II oxidation state due to stabilization by the π-bonded arene ligands [35], the studied organometallic complexes with aminomethyl(diphenyl)phosphanes of fluoroquinolones are prone to undergo electrochemical processes. Taking into consideration the potential values for oxidation of Ru(II) ion it can be supposed that investigated complexes can participate in redox chemistry inside cells, as the required redox potential window is estimated to be −0.4 to +0.8 V *vs* NHE [36]. This may result in strengthening the production of reactive oxygen species and in consequence lead to irreversible changes in cellular redox equilibrium, that end in cell death.

3.3. Interactions with CT-DNA

Knowing that DNA is a potential target for transition metal anticancer complexes [6, 37, 38], we investigated the binding profiles of studied ruthenium(II) complexes to calf thymus DNA (CT-DNA) in order to provide insight into their mechanism of action. Fluorescence spectroscopy was used to study kinetics of interactions between CT-DNA and studied ruthenium(II) complexes. To achieve this, the fluorescence spectra of complexes in the absence and presence of CT-DNA at different concentrations were recorded. Stern-Volmer plots, obtained by titration of CT-DNA-EB system with Ru(II) complexes in molar ratios 1:1:1, 1:1:2, 1:1:5, 1:1:10 and 1:1:20 (CT-DNA:EB:Ru) after 1 hour incubation time, are presented in Fig. 4.

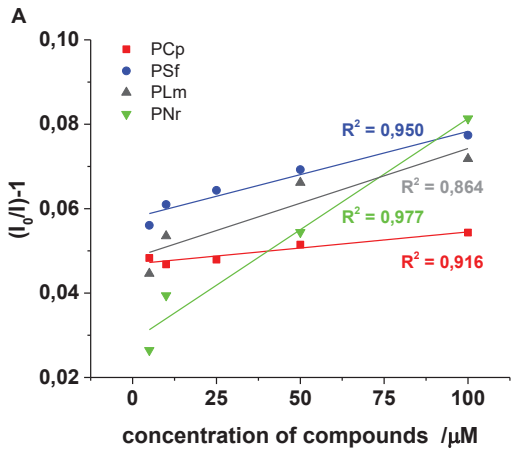

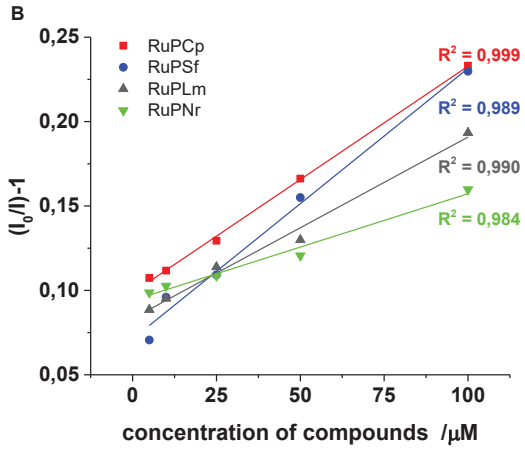

Fig. 4. Stern–Volmer plots of the CT DNA–EB system quenched by (A) **PCp**, **PSf**, **PLm**, **PNr**, and (B) **RuPCp**, **RuPSf**, **RuPLm**, **RuPNr**. I_0 and I – intensity of CT DNA–EB in the absence and presence of the increasing concentration of the compounds [μM].

Upon addition of CT-DNA to ligands or the corresponding Ru(II) complexes, a considerable decrease in fluorescence was observed without significant changes in the wavelength of CT transition for complexes. Stern-Volmer plots for all of the phosphanes (**PCp**, **PSf**, **PLm**, and **PNr**), and ruthenium(II) complexes (**RuPCp**, **RuPSf**, **RuPLm**, **RuPNr**) are linear, what proves dynamic mechanism of interactions between DNA and studied compounds and confirms their intercalating properties. Observed fluorescence quenching of CT-DNA-EB complex clearly indicates that new studied "piano-stool" ruthenium(II) compounds are able to intercalate between DNA base pairs. Ru(II) complexes are more effective intercalators than the corresponding phosphines due to lower values of I/I_0 at the end of incubation time (SI, Fig. S10) and higher values of slope factors of Stern–Volmer dependencies (Fig. 4). The strength of the ligands' and complexes' intercalation with CT-DNA, expressed by K_{sv} values, is shown in Table 1.

Table 1

Determined K_{sv} values for the studied phosphanes and studied Ru(II) complexes.

	K_{SV} [M^{-1}]		
PCp	7.62×10^1	**RuPCp**	1.34×10^3
PSf	2.05×10^2	**RuPSf**	1.60×10^3
PLm	2.59×10^2	**RuPLm**	1.07×10^3
PNr	5.27×10^2	**RuPNr**	6.32×10^2

Interestingly, in-depth analysis of Stern–Volmer plots leads to conclusion, that from the point of view of more efficient interactions with CT-DNA, the presence of the cyclopropane substituent in the antibiotic structure of coordinated phosphine ligand plays a crucial role. This conclusion is drawn based on K_{sv} values, which are 1.34×10^3 M^{-1} and 6.32×10^2 M^{-1} for **RuPCp** and **RuPNr**, respectively. The same dependence of values was observed for the corresponding phosphines (*vide supra*, Table 1). Whereas, substituents in piperazine structure did not influence intercalation properties of studied half-sandwich Ru(II) complexes modified with phosphane derivatives of fluoroquinolones, as there are not significant difference in K_{sv} values for **PSf** and **PLm** ligands, as well as for **RuPSf** and **RuPLm** complexes (*vide supra*, Table 1, Fig 1).

Moreover, circular dichroism (CD) spectroscopy demonstrated that the investigated **RuPCp**, **RuPSf**, **RuPLm**, **RuPNr** complexes did not cause the conformational changes in CT-DNA structure. After CT-DNA titration by Ru(II) complexes no noticeable changes in CD spectra were observed (SI, Fig. S11), indicating binding to DNA by coordination or destruction its superhelical conformation, in similarity to the corresponding phosphanes (**PCp**, **PSf**, **PLm**, and **PNr**) [11]. These findings suggest intercalation or surface interaction involving π-stacking interactions between the complex and the DNA base pair.

3.4. pBR322 plasmid damage

In order to get more information on a direct DNA–metal interaction of studied ruthenium(II) complexes we decided to study the alteration of DNA structure by the electrophoretic mobility of different forms of DNA plasmid on agarose gels (Fig. 5).

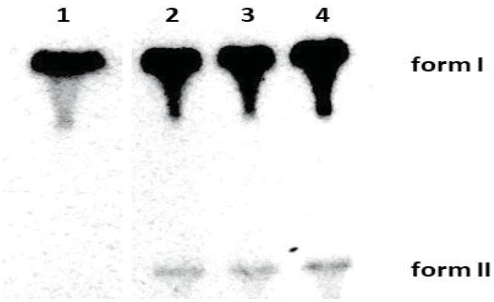

Fig. 5. Selected agarose gel electrophoresis of *pBR322* plasmid cleavage by half sandwich ruthenium(II) complex with aminomethylphosphines derived from ciprofloxacine in the 10% DMF solution. Lanes: 1 – plasmid (control); 2 – plasmid + 60 μM **RuPCp**; 3 – plasmid + 80 μM **RuPCp**; 4 – plasmid + 100 μM **RuPCp**.

When *pBR322* plasmid was incubated with increasing concentrations of **RuPCp** an increase of the relaxed open circular form of the plasmid (form II) was observed, that was found to correlate inversely with the amount of the supercoiled form (form I). This clearly indicates that since a direct conversion of the form I into the form II is taking place, thus the studied complexes are able to cause a single-strain plasmid cleavage. It can also be supposed that investigated complexes are not capable of a double-strain plasmid damage leading to formation of a linear form of the plasmid (form III), which is not observed in the gel electrophoresis of *pBR322* plasmid (Fig. 5). It is worth mentioning that the corresponding ligands alone (**PCp**, **PSf**, **PLm**, and **PNr**), even though they exhibited slight interactions with CT-DNA (*vide supra*, Fig. 4), did not cause any DNA degradation [11]. Our findings are in agreement with work of Romerosa *et al.*, who also observed formation of open circular form of plasmid resulting from not selective interactions of cyclopentadienidoruthenium(II) complexes bearing water-soluble phosphanes with nucleobases within intra- or inter-strand crosslinking. The authors suggested that piano-stool Ru(II) complexes can be active DNA agents acting by both mechanisms – with or without phosphine ligand dissociation (non-dissociative or dissociative mechanism, respectively) [29].

3.5. Polymeric micelles

The emergence of selective and efficient delivery of highly hydrophobic drugs into living system has intensified the need for their encapsulation inside drug delivery systems, for instance polymeric micelles, liposomes, and other more sophisticated supramolecular assemblies [15, 39-42]. The versatility of polymeric micelles produced from amphiphilic copolymers offers variety of self-assembled nanostructures with diverse morphology and size

in the range between 10 to 200 nm [39]. This results in significant advances in biomedical area due to their varying functions and clinical applications. Furthermore, this strategy enables to reduce systemic toxicity by enhancing passive accumulation in the tumor tissue due to the enhanced permeability and retention (EPR) effect [43-45].

Furthermore, since most of the ruthenium(II) complexes are not sufficiently soluble in water, therefore DMSO or DMF has to be usually used as solubilizing agent. However, this often leads to the solvolysis of the ruthenium(II) complexes, as shown recently for instance for [Ru(η^6-arene)Cl_2(L)] complexes (L = N-heterocyclic ligands) [46]. In consequence, solvolised ruthenium(II) complex may exhibit totally different activity *in vitro* in comparison to a parent dichlorido compound. In the case of the half-sandwich ruthenium(II) complex **RuPP$_1$**, studied by us previously and treated as the parent complex, we observed that this complex was susceptible to decomposition [10]. Thus, in order to avoid solvolysis of metal complexes various delivery systems such as mentioned above formulations loaded with these complexes have been currently proposed. Concluding, justification of application of drug delivery systems for highly active anticancer compounds lies not only in prevention of hydrolysis or solvolysis, but also in precise accumulation in the target tumor tissue, drug release, and selective local application [8].

Accordingly to all above-mentioned and due to poor solubility of studied ruthenium(II) complexes in water we decided to encapsulate two complexes (**RuPCp** and **RuPNr**) into polymeric micelles made of Pluronic P-123 (PEO-PPO-PEO triblock copolymer), using thin-film hydration method [47]. **RuPCp** and **RuPNr** were selected consciously because of differences in the structure of coordinated fluoroquinolones (cyclopropyl and ethyl moiety in quinolone, respectively). This presumably resulted in the strongest and the weakest interaction with CT-DNA for **RuPCp** and **RuPNr**, respectively (*vide supra*, Fig. 4). Apparently, these complexes should also exhibit different biological activity *in vitro*. TEM images of selected Pluronic P-123 micelles with encapsulated **RuPNr** complex (**RuPNr_M**) with statistical analysis of size (ImageJ) are presented in Fig. 6.

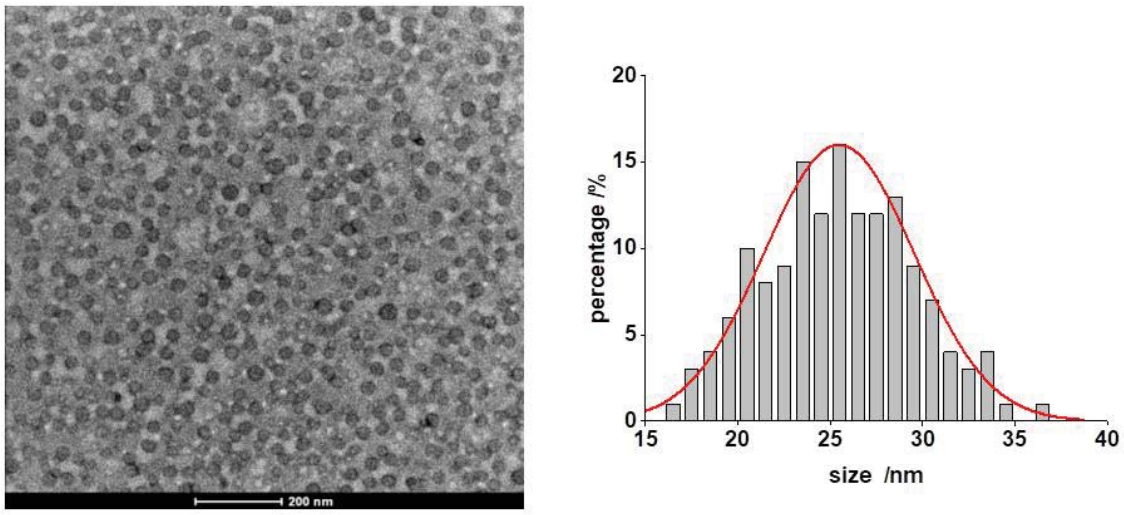

Fig. 6. TEM images of Pluronic P-123 formulation with encapsulated **RuPNr** complex (**RuPNr_M**) with statistical analysis of size (ImageJ).

Negative staining TEM images revealed spherical shape and smooth surface forming homogeneous polymeric micelles with a size in agreement with DLS data (Table 2).

Table 2

Hydrodynamic diameter determined by DLS technique, loading content and encapsulation efficiency for selected Pluronic P-123 formulation.

formulation	hydrodynamic diameter [nm]	LC ± S.D. [%]	EE ± S.D. [%]
P-123_M	22 ± 8 PDI 0.5 ± 0.1	-	-
RuPCp_M	26 ± 5 PDI 0.4 ± 0.1	3.9 ± 3.1	96.3 ± 1.5
RuPNr_M	26 ± 3 PDI 0.4 ± 0.1	9.3 ± 3.5	94.0 ± 0.2

Drug loading content (LC) and encapsulation efficiency (EE) were assessed with application of ICP-MS technique (Table 2). In the case of both studied complexes the determined LC and EE values prove effective and efficient loading of the Ru(II) complexes inside the Pluronic P-123 micelles, what will ensure their effective delivery. The mean micelle size of **RuPCp_M** and **RuPNr_M** was less than 50 nm, which is smaller than the critical size required to avoid capture by the reticuloendothelial system (RES). In view of the

determined small size of the Pluronic P-123 micelles loaded with **RuPCp** or **RuPNr** complexes (*ca.* 25 nm), it is plausible that such nanoformulations will facilitate ruthenium(II) complexes accumulation into tumor tissues combining the avoidance of the RES system with the EPR effect and low steric hindrance. Zeta potential of stable **RuPNr_M** micelles was equal to be –1.59 ± 0.33 mV (pH = 7.4), resulting from slightly negative potential of uncharged PEO amphiphilic copolymers [48]. Given low value indicates the tendency to aggregation of synthesized micelles, what is beneficial for accelerating of drug release. As the polymeric micelles enter the tumor cells (*vide infra*, Fig. 8 and 9), it can be supposed that in pathological tumor microenvironment, characterized by lower pH (*e.g.*, pH = 5.5 for endosome, pH = 5.0 for lysosome), when compared with normal tissues (pH = 7.4), efficient release of Ru(II) complexes will be facilitated. This will be realized mainly due to the fact that such Pluronic P-123 nanoformulations tend to form aggregates releasing their load in dependence to pH, as observed also by other authors [47].

3.6. Cytotoxicity study in vitro

Herein, the cytotoxicity of two particular polymeric formulations **RuPCp_M** and **RuPNr_M** was studied on selected cell line – an lung adenocarcinoma cells (A549 cell line). The cell viability was assessed by MTT assay after 24 hours incubation with studied formulations and additional 24h for recovery time in free media (Table 3).

Table 3

IC50 values [μM] for A549 cell line determined after 24h incubation with **RuPCp_M** and **RuPNr_M** and additional 24h for recovery time in free media.

	A549 cell line (24h)
formulation	**IC50 ± SD [μM]**
RuPCp_M	39.5 ± 9.3
RuPNr_M	77.1 ± 2.7

As shown in Table 3, both **RuPCp_M** and **RuPNr_M** exhibited high cytotoxicity towards studied human cancer cells, when compared with the earlier studied by our group organometallic ruthenium(II) complexes with aminomethylphospanes derived from morpholine or piperazine and not bearing fluoroquinolones' moieties. What is noteworthy, the determined IC50 values are one order of magnitude higher than in the case of the latter complexes and cisplatin [10]. Notably, **RuPCp_M** displayed higher cytotoxicity than

RuPNr_M *in vitro*, what corresponds to their higher affinity of the DNA-binding showed in the model study on CT-DNA interactions (*vide supra*, Fig 4).

Cellular morphology after treatment with studied micelles was visualized *via* microscopy, including fluorescent imaging after adequate dye staining with acridine orange (AO) and propidium iodide (PI) (Fig. 7).

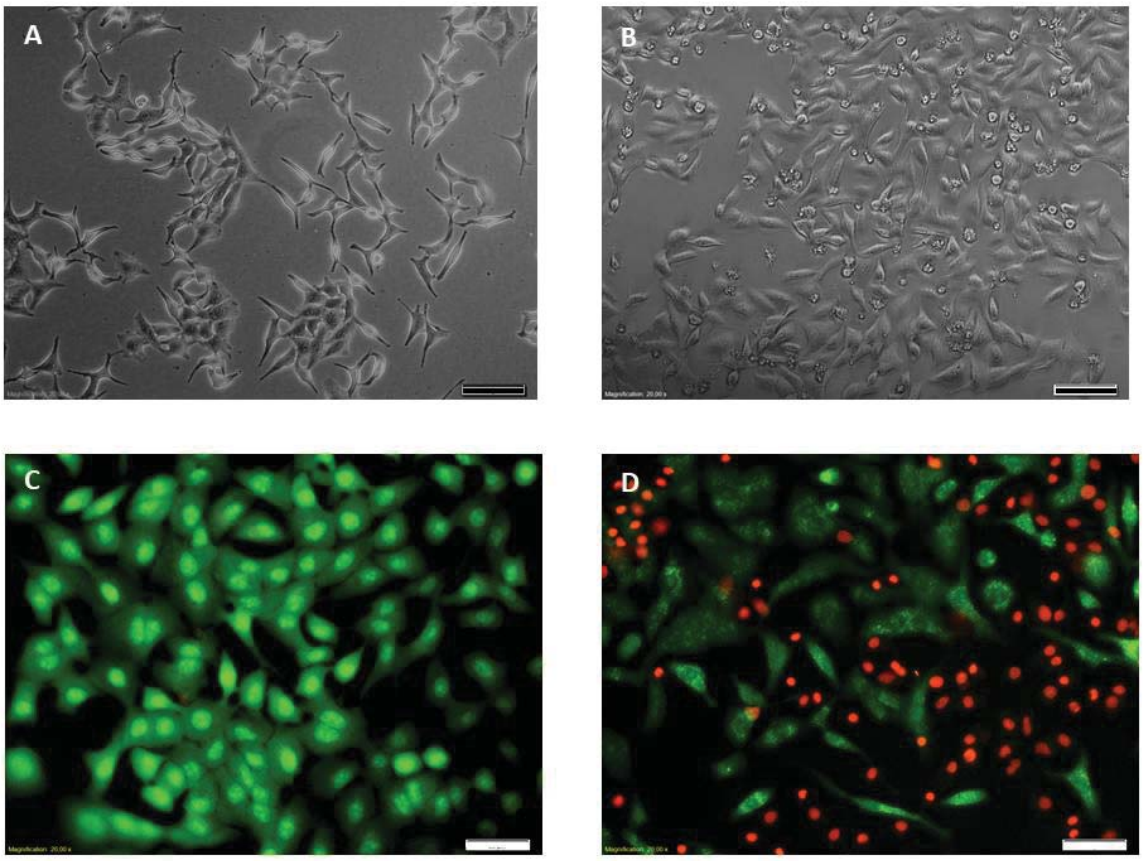

Fig. 7. Visible light and fluorescent images presenting A549 cells: (A, C) untreated (control) and (B, D) treated with **RuPCp_M** formulation for 24 hours at IC50 concentration. Cells after treatment were stained with acridine orange (green, viable cells) and propidium iodide (red, dead cells). Bar – 50 μm

AO is a vital dye, which stains both live and dead cells, while PI stains only cells that have lost membrane integrity. Analysis of fluorescence images revealed significant changes in cell morphology, indicating number of viable (green, AO+) and dead (red, PI+) cells. While, untreated control cells appeared uniformly green with spindle-shape.

3.7. Cellular uptake

One of the major goals in the development of novel metal-based anticancer drug candidates is to obtain an efficient uptake of a compound into tumor cells, while presenting increased therapeutic efficacy and decreased cytotoxicity in the case of healthy tissue. Confocal microscopy was applied to confirm cellular uptake of studied **RuPCp_M** and **RuPNr_M** formulations (Fig. 8).

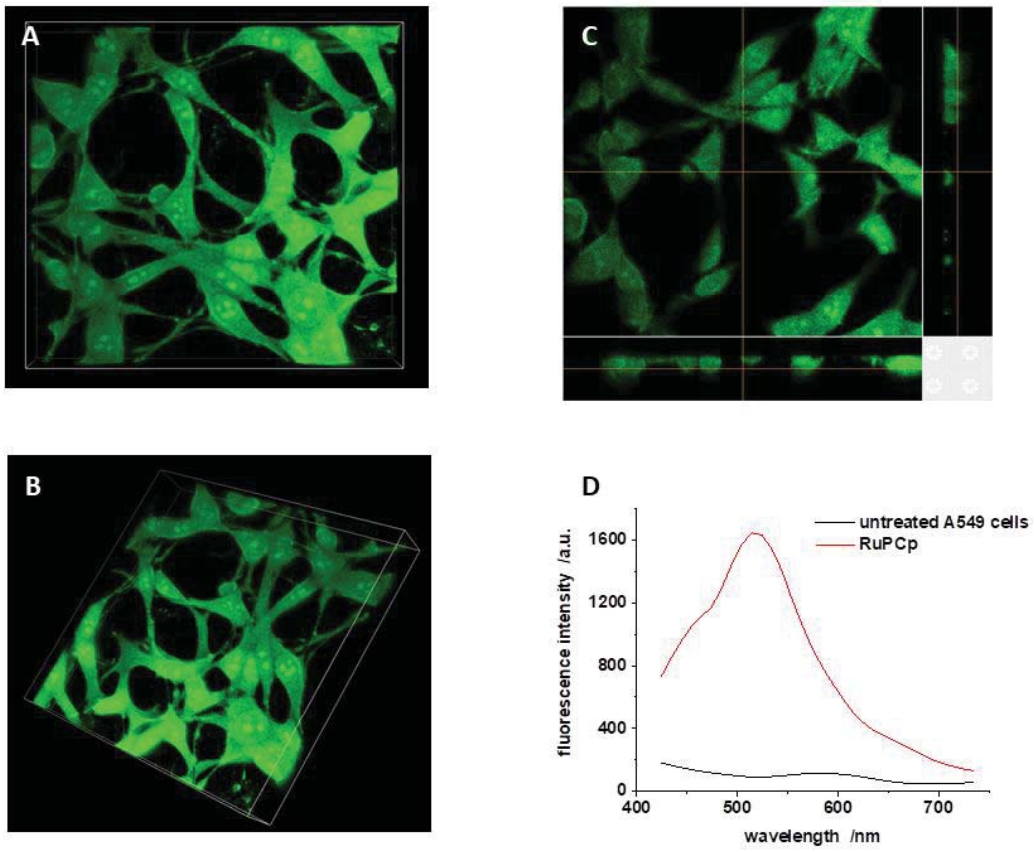

Fig. 8. Confocal microscopy. (A) and (B) selected 3D images of A549 cells after 4h incubation with **RuPCp_M** at IC50 in different positions (magnification 60.00×, ex = 358 nm), (C) cross-sectional image, and (D) emission spectra of cells after treatment and control cells (untreated A549 cells).

Confocal microscopy confirms unquestionably cellular uptake of **RuPCp_M** and **RuPNr_M** formulations. This is proved by analysis of the cross-sectional images and emission spectra of the tested compounds, that penetrated into the cells. Non-differing in intensity emission from the compounds was visible inside the whole cell, what indicates their uniform distribution throughout the cells and no favorable accumulation in any cellular compartments or organelles.

Furthermore, to assess how efficiently micelles loaded with ruthenium(II) compounds were taken up by A549 cells, the cellular accumulation of Ru ion was detected using ICP-MS technique after cell treatment with 2 μM **RuPCp_M** or **RuPNr_M** for 4 and 24 hours (Fig. 9).

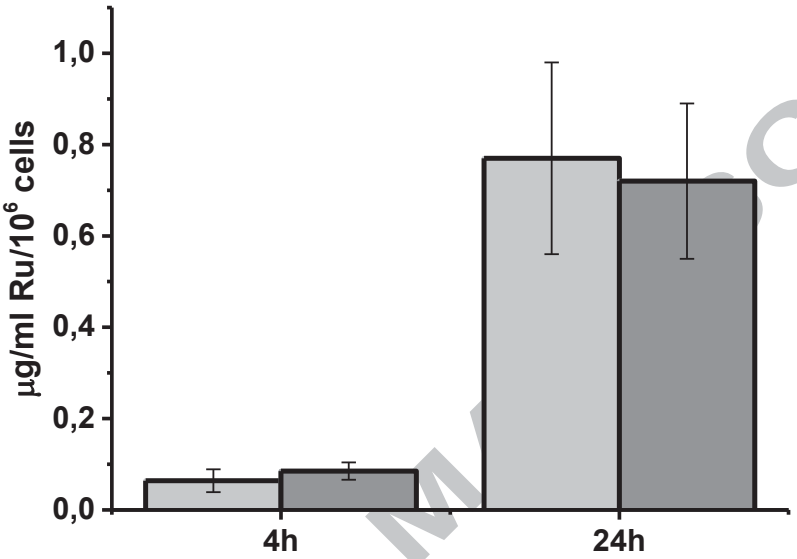

Fig. 9. Intracellular ruthenium accumulation expressed by μg/ml Ru per 10^6 cells after 4 and 24 hours of A549 cell incubation with 2 μM **RuPCp_M** or **RuPNr_M**.

Time-depending cellular uptake of **RuPCp_M** and **RuPNr_M** was determined to be 0.77 ± 0.21 μg/ml Ru/10^6 cells and 0.72 ± 0.17 μg/ml Ru/10^6 cells, respectively following long-term treatment (24h). This indicates significantly increased accumulation of Ru(II) complexes, when compared with studied previously counterparts with aminomethylphospanes derived from piperazine not bearing fluoroquinolone's motif, as reported previously [10]. These results, together with confocal analysis, clearly support an enhanced pattern of cellular uptake into A549 cells of micellar nanocarriers containing the studied organometallic ruthenium(II) complexes. It can be concluded that successful and efficient uptake of poorly soluble half-sandwich Ru(II) complexes is observed mainly because of the interesting feature of Pluronic P-123, which is capable to interact with cell membranes, leading to decreased microviscosity, pore formation on the membrane and accelerated transmembrane drug translocation [47].

3.8. Comet assay

Several mechanisms have been proposed to elucidate the anticancer activities of ruthenium complexes: (*i*) interaction with DNA, *(ii*) blocking of the cell cycle, (*iii*) inhibition of various kinases, (*iv*) inhibition of topoisomerases, and (*v*) induction of mitochondrial dysfunction pathway [1]. To gain more insight into the underlying mechanism of cytotoxicity induced by nanoformulation containing selected Ru(II) complex (**RuPCp_M**), induction of DNA damage, which is considered as hallmark of apoptosis, was investigated. The single-cell gel electrophoresis (comet assay) is an effective and simple measure for evaluating the DNA integrity, since a cell with damaged DNA stained with EB, subjected to electrophoresis, appears as a comet like.

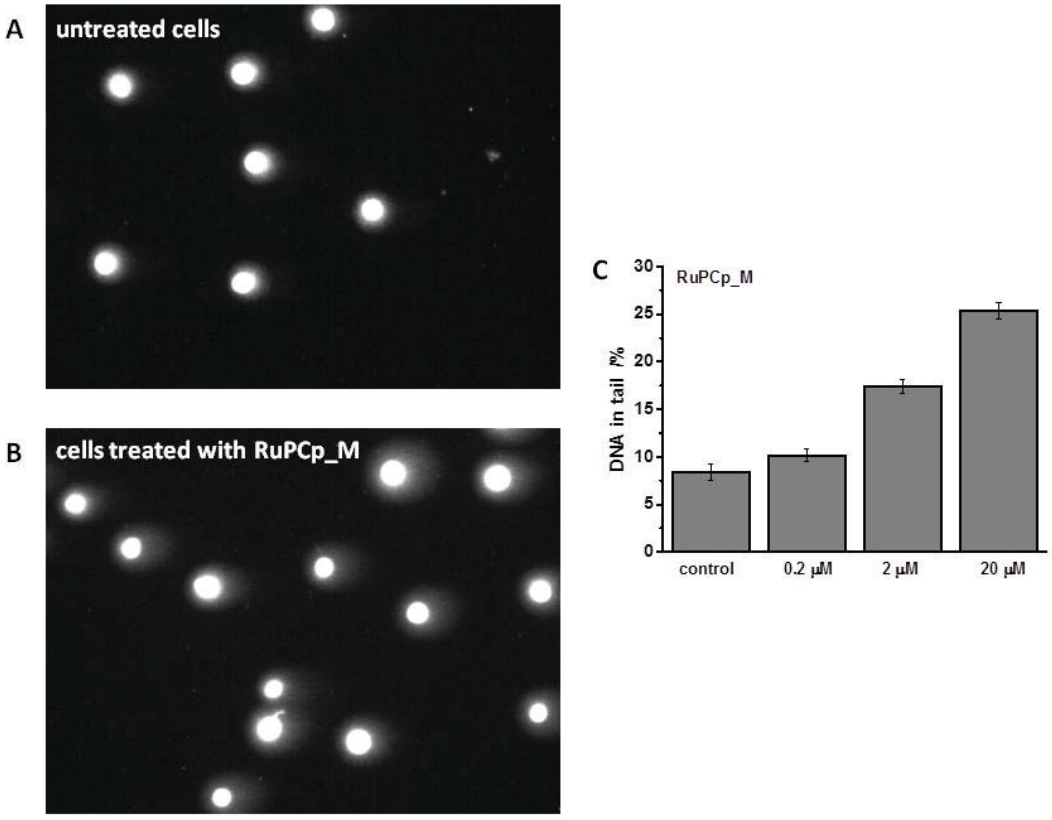

Fig. 10. Comet assay analysis of DNA damage. Representative images of (**A**) A549 untreated cells (control) and (**B**) cells after 24h treatment with **RuPCp_M** formulation (20 µM **RuPCp**). (**C**) DNA damage presented as the mean value of the percentage of DNA in the comet tail (DNA in tail %) with increasing concentration of **RuPCp**. Given concentrations refers to **RuPCp** complex encapsulated inside micelles. Images were made using the computer program Comet Plus (Theta System GmbH, Germany).

As shown in Fig. 10 in the control (untreated cells), the percentage of DNA in the comet tail was found to be at *ca.* 8%. After the treatment of A549 cells with the increasing concentration of **RuPCp** complex for 24 hours (introduced into cells in **RuPCp_M**), the statistically significant and well-formed comet like was observed. The length of tail indicated the extent of *ca.* 26% of DNA damage. These results identify the studied complex can lead to DNA damage in A549 cells, which is an undoubted hallmark of apoptotic cell death, mitotic catastrophe or both [49]. Importantly, based on these findings along with, in particular, interactions with CT-DNA and *pBR322* plasmid (intercalating properties, cleavage of DNA helix), it can be supposed that studied arene Ru(II) complexes arrest cells for DNA repair resulting in irreversible DNA damage and subsequent cell death. It is well-known that DNA damage can be caused not only by direct interactions of chemotherapeutics with nucleic acid double helix but also by other mechanisms such as ROS-mediated DNA cleavage. First of all, our research shows that the mechanism associated with the generation of ROS can not be rejected. In addition, other molecular pathways affecting the increase of DNA damage such as mitochondrial activation of apoptosis should also be taken into account. Thus, more precise investigation focused on elucidation of molecular mode of action of studied piano-stool ruthenium(II) complexes with phosphane derivatives of fluoroquinolones is required.

4. Conclusions

In this paper, we explored the potential of Pluronic P-123 micelles as suitable nanocarriers to deliver two selected ruthenium(II) compounds **RuPCp** and **RuPNr**, allowing to maintain their activity and mechanism of action. Studied functionalities such as micelle stability, micellar size distribution, drug loading capacity, and high cytotoxic index towards cancer cells provide with possible application of these polymeric nanosystems for selective and efficient delivery of anticancer drugs *i.e.*, organometallic Ru(II) complexes with phosphine derivatives of fluoroquinolones. What is noteworthy, determined small size of prepared micelles (*ca.* 25 nm) and high drug loading efficiency (*ca.* 95%) ideally meets crucial design criteria for an effective penetration into the tissue (proved by confocal microscopy). Presumably, this will provide stealth against mononuclear phagocyte system (MPS) for sufficient longer circulation and better accumulation in the target tissue. Importantly, based on electrochemical characterization of all studied complexes we postulate their participation in intracellular redox processes connected with ROS generation. Furthermore, study on interactions with macromolecules (CT-DNA, *pBR322* plasmid)

revealed: (*i*) intercalating properties of investigated arene Ru(II) complexes, and (*ii*) possibility to induce a single strand DNA cleavage. Irreversible DNA fragmentation was also confirmed by single cell gel electrophoresis (comet assay) in an agarose gel matrix. In light of these results it may be supposed that prepared FDA-proved polymeric nanoformulations containing arene Ru(II) complexes with aminomethyl(diphenyl)phosphine derived from fluoroloquinolones will assure safe biodegradability for easy elimination from the body, targetability for therapeutic efficacy, tunable stability, improved pharmacokinetics and pharmacodynamic profiles. Finally, reproducibility along with facile and inexpensive method of synthesis will be also guaranteed.

Acknowledgments

The research was carried out with the equipment purchased thanks to the financial support of the European Regional Development Fund in the Framework of the Polish Innovation Economy Operational Program (contract no. POIG.02.01.00-12-023/08). The authors gratefully acknowledge financial support from the Polish National Science Centre (Grant 2011/03/B/ST5/01557). Electrochemical characterization of studied complexes were carried out thanks to the financial support from the Polish National Science Centre (Grant 2017/01/X/NZ7/01148). The authors are grateful to Marcin Kobielusz, PhD, from Jagiellonian University in Kraków for helpful and comprehensive discussions on electrochemical characterization of studied complexes. The authors would like also to acknowledge Professor Mariusz Kępczyński from Jagiellonian University in Kraków for confocal imaging. CIBER-BBN is an initiative funded by the VI National R&D&i Plan 2008-2011 financed by the Instituto de Salud Carlos III with the assistance of the European Regional Development Fund.

Appendix A. Supplementary material

Supplementary data associated with this article can be found, in the online version, at ….

References

[1] P. Zhang, P.J. Sadler, Advances in the design of organometallic anticancer complexes, Journal of Organometallic Chemistry, 839 (2017) 5-14.

[2] J. Arshad, M. Hanif, S. Movassaghi, M. Kubanik, A. Waseem, T. Söhnel, S.M.F. Jamieson, C.G. Hartinger, Anticancer Ru(η6-p-cymene) complexes of 2-pyridinecarbothioamides: A structure–activity relationship study, Journal of Inorganic Biochemistry 177 (2017) 395-401.

[3] R.H. Berndsen, A. Weiss, A. U.K., T.J. Wong, P. Meraldi, A.W. Griffioen, P.J. Dyson, P. Nowak-Sliwinska, Combination of ruthenium(II)-arene complex [Ru(η6-p-cymene)Cl_2(pta)] (RAPTA-C) and the epidermal growth factor receptor inhibitor erlotinib results in efficient angiostatic and antitumor activity, Scientific Reports, 7 (2017) 1-16.

[4] R.G. Teixeira, A.R. Bras, L. Leonor Corte-Real, R. Tatikonda, A. Sanches, M.P. Robalo, F. Avecilla, T. Moreira, M.H. Garcia, M. Haukka, A. Preto, A. Valente, Novel ruthenium methylcyclopentadienyl complex bearing a bipyridine perfluorinated ligand shows strong activity towards colorectal cancer cells, European Journal of Medicinal Chemistry, 143 (2018) 503-514.

[5] P. Sathyadevi, P. Krishnamoorthy, N.S.P. Bhuvanesh, P. Kalaiselvi, V.V. Padma, N. Dharmaraj, Organometallic ruthenium(II) complexes: Synthesis, structure and influence of substitution at azomethine carbon towards DNA/BSA binding, radical scavenging and cytotoxicity, European Journal of Medicinal Chemistry, 55 (2012) 420-431.

[6] T. Tsolis, K.D. Papavasileiou, S.A. Divanis, V.S. Melissas, A. Garoufis, How half sandwich ruthenium compounds interact with DNA while not being hydrolyzed; a comparative study, Journal of Inorganic Biochemistry, 160 (2016) 12-23.

[7] L. Zeng, P. Gupta, Y. Chen, E. Wang, L. Ji, H. Chao, Z.S. Chen, The development of anticancer ruthenium(II) complexes: from single molecule compounds to nanomaterials, Chem. Soc. Rev., 46 (2017) 5771-5804

[8] D. Edeler, S. Arlt, V. Petkovic, G. Ludwig, D. Dracac, D. Maksimovic-Ivanic, S. Mijatovic, G.N. Kaluderovic, Delivery of [Ru(η6-p-cymene)Cl2{Ph2P(CH2)3SPh-κP}] using unfunctionalized and mercapto functionalized SBA-15 mesoporous silica: Preparation, characterization and in vitro study, Journal of Inorganic Biochemistry, 180 (2018) 155-162.

[9] J.H. Gong, X.J. Liu, B.Y. Shang, S.Z. Chen, Y.S. Zhen, HERG K+ channel related chemosensitivity to sparfloxacin in colon cancer cells, Oncol Rep., 23 (2010) 1747-1756.

[10] M. Płotek, R. Starosta, U.K. Komarnicka, A. Skórska-Stania, P. Kołoczek, A. Kyzioł, Ruthenium(II) piano stool coordination compounds with aminomethylphosphanes: Synthesis, characterisation and preliminary biological study in vitro, Journal of Inorganic Biochemistry, 170 (2017) 178-187.

[11] U.K. Komarnicka, R. Starosta, M. Płotek, R.F.M. de Almeida, M. Jeżowska-Bojczuk, A. Kyzioł, Copper(I) complexes with phosphine derived from sparfloxacin. Part II: a first insight into the cytotoxic action mode, Dalton Trans., 45 (2016) 5052-5063.

[12] U.K. Komarnicka, R. Starosta, A. Kyzioł, M. Płotek, M. Puchalska, M. Jeżowska-Bojczuk, New copper(I) complexes bearing lomefloxacin motif: spectroscopic properties, in vitro cytotoxicity and interactions with DNA and human serum albumin, Journal of Inorganic Biochemistry, 165 (2016) 25-35.

[13] A. Kyzioł, A. Cierniak, J. Gubernator, A. Markowski, M. Jeżowska-Bojczuk, U.K. Komarnicka, Copper(I) complexes with phosphine derived from sparfloxacin. Part III: multifaceted cell death and preliminary study of liposomal formulation of selected copper(I) complex, Dalton Trans., accepted (2018).

[14] A. Bykowska, U.K. Komarnicka, M. Jeżowska-Bojczuk, A. Kyzioł, CuI and CuII complexes with phosphine derivatives of fluoroquinolone antibiotics - a comparative study on the cytotoxic mode of action, J. Inorg. Biochem., (2018).

[15] M. Cagel, F.C. Tesan, E. Bernabeu, M.J. Salgueiro, M.Z. Zubillaga, M.A. Moretton, D.A. Chiappetta, Polymeric mixed micelles as nanomedicines: Achievements and perspectives, European Journal of Pharmaceutics and Biopharmaceutics, 113 (2017) 211-228.

[16] I. Romero-Canelon, B. Phoenix, A. Pitto-Barry, J. Tran, J.J. Soldevila-Barreda, N. Kirby, S. Green, P.J. Sadler, N.P.E. Barry, Arene ruthenium dithiolatoecarborane complexes for boron neutron capture therapy (BNCT), Journal of Organometallic Chemistry, 796 (2015) 17-25.

[17] X. Duan, D. Liu, C. Chan, W. Lin, Polymeric micelle-mediated delivery of DNA-targeting organometallic complexes for resistant ovarian cancer treatment, Small, 11 (2015) 3962-3972.

[18] B.M. Blunden, A. Rawal, H. Lu, M.H. Stenzel, Superior Chemotherapeutic Benefits from the Ruthenium-Based Anti-Metastatic Drug NAMI-A through Conjugation to Polymeric Micelles, Macromolecules, 47 (2014) 1646−1655.

[19] W. Sun, M. Parowatkin, W. Steffen, H.J. Butt, V. Mailander, S. Wu, Ruthenium-Containing Block Copolymer Assemblies: Red-Light-Responsive Metallopolymers with Tunable Nanostructures for Enhanced Cellular Uptake and Anticancer Phototherapy, Adv. Healthcare Mater., 5 (2016) 467-473.

[20] W. Sun, S. Li, B. Haupler, J. Liu, S. Jin, W. Steffen, U.S. Schubert, H.J. Butt, X.J. Liang, S. Wu, An Amphiphilic Ruthenium Polymetallodrug for Combined Photodynamic Therapy and Photochemotherapy In Vivo, Adv. Mater., 29 (2017) 1603702.

[21] W. Sun, X. Zeng, Photoresponsive ruthenium-containing polymers: potential polymeric metallodrugs for anticancer phototherapy, Dalton Trans., 47 (2018) 283-286.

[22] U.K. Komarnicka, R. Starosta, K. Guz-Regner, G. Bugla-Płoskońska, A. Kyzioł, M. Jeżowska-Bojczuk, Phosphine derivatives of sparfloxacin – Synthesis, structures and in vitro activity, Journal of Molecular Structure, 1096 (2015) 55-63.

[23] Agilent, CrysAlis PRO, Agilent Technologies Ltd., Yarnton, Oxfordshire, England, (2015).

[24] G.M. Sheldrick, Crystal structure refinement with SHELXL Acta Crystallogr., C71 (2015) 3-8.

[25] Mercury 3.9.

[26] L.R.V. Favarin, P.P. Rosa, L. Pizzuti, A. Machulek Jr, A.R.L. Caires, L.S. Bezerra, L.M.C. Pinto, G. Maia, C.C. Gatto, D.F. Back, A. dos Anjos, G.A. Casagrande, Synthesis and structural characterization of new heteroleptic copper(I) complexes based on mixed phosphine/thiocarbamoyl-pyrazoline ligands, Polyhedron, 121 (2017) 185-190.

[27] M. Płotek, R. Starosta, U.K. Komarnicka, A. Skórska-Stania, G. Stochel, A. Kyzioł, New ruthenium(II) coordination compounds possessing bidentate aminomethylphosphane ligands: synthesis, characterisation and biological study *in vitro*, Dalton Transactions, 44 (2015) 13969-13978.

[28] C.S. Allardyce, P.J. Dyson, D.J. Ellis, P.A. Salter, R. Scopelliti, Synthesis and characterisation of some water soluble ruthenium(II)-arene complexes and an investigation of

their antibiotic and antiviral properties, Journal of Organometallic Chemistry, 668 (2003) 35-42.

[29] A. Romerosa, M. Saoud, T. Campos-Malpartida, C. Lidrissi, M. Serrano-Ruiz, M. Peruzzini, J.A. Garrido, F. García-Maroto, DNA Interactions Mediated by Cyclopentadienidoruthenium(II) Complexes Containing Water-Soluble Phosphanes, Eur. J. Inorg. Chem., (2007) 2803-2812.

[30] L. Colina-Vegas, W. Villarreal, M. Navarro, C. Rodrigues de Oliveira, A.E. Graminha, P.I. da S. Maia, V.M. Deflon, A.G. Ferreira, M.R. Cominetti, A.A. Batista, Cytotoxicity of Ru(II) piano–stool complexes with chloroquine and chelating ligands against breast and lung tumor cells: Interactions with DNA and BSA, Journal of Inorganic Biochemistry, 153 (2015) 150-161.

[31] L. Colina-Vegasa, L. Luna-Dulcey, A.M. Plutín, E.E. Castellano, M.R. Cominetti, A.A. Batista, Half sandwich Ru(II)-acylthioureas complexes: DNA/HSA-binding, antimigration and cell death properties in a breast tumor cell line, Dalton Trans., 46 (2017) 12865-12875.

[32] L. Diebold, N.S. Chandel, Mitochondrial ROS regulation of proliferating cells, Free Radical Biology and Medicine, 100 (2016) 86-93.

[33] N.K. Kumar, G. Venkatachalam, R. Ramesh, Y. Liu, Half-sandwich para-cymene ruthenium(II) naphthylazophenolato complexes: Synthesis, molecular structure, light emission, redox behavior and catalytic oxidation properties, Polyhedron, 27 (2008) 157-166.

[34] C. Pettinari, M.A. Cerquetella, R. Pettinari, M. Monari, T.C.O. Mac Leod, L.M.D.R.S. Martins, A.J.L. Pombeiro, Coordination Chemistry of the (η6-p-Cymene)ruthenium(II) Fragment with Bis-, Tris-, and Tetrakis(pyrazol-1-yl)borate Ligands: Synthesis, Structural, Electrochemical, and Catalytic Diastereoselective Nitroaldol Reaction Studies, Organometallics, 30 (2011) 1616-1626.

[35] B. Therrien, Functionalised η6-arene ruthenium complexes, Coordination Chemistry Reviews, 253 (2009) 493-519.

[36] U. Jungwirth, C.R. Kowol, B.K. Keppler, C.G. Hartinger, W. Berger, P. Heffeter, Anticancer Activity of Metal Complexes: Involvement of Redox Processes, Antioxid Redox Signal, 15 (2011) 1085-1127.

[37] S. Nikolic, L. Rangasamy, N. Gligorijevic, S. Arandelovic, S. Radulovic, G. Gasser, S. Grguric-Sipka, Synthesis, characterization and biological evaluation of novel Ru(II)–arene complexes containing intercalating ligands, Journal of Inorganic Biochemistry, 160 (2016) 156-165.

[38] Y. Chen, Q. Wu, X. Wang, Q. Xie, Y. Lan, W. Mei, Microwave-Assisted Synthesis of Arene Ru(II) Complexes Induce Tumor Cell Apoptosis Through Selectively Binding and Stabilizing bcl-2 G-Quadruplex DNA, Materials, 9 (2016) 1-14.

[39] A.S. Deshmukh, P.N. Chauhan, M.N. Noolvi, K. Chaturvedi, K. Ganguly, S.S. Shukla, M.N. Nadagouda, T.M. Aminabhavi, Polymeric micelles: Basic research to clinical practice, International Journal of Pharmaceutics, 532 (2017) 249-268.

[40] M. Marguet, C. Bonduelle, S. Lecommandoux, Multicompartmentalized polymeric systems: towards biomimetic cellular structure and function, Chem. Soc. Rev., 42 (2013) 512--529.

[41] E. Nogueira, A.C. Gome, A. Preto, A. Cavaco-Paulo, Design of liposomal formulations for cell targeting, Colloids and Surfaces B: Biointerfaces, 136 (2015) 514-526.

[42] E. Pérez-Herrero, A. Fernández-Medarde, Advanced targeted therapies in cancer: Drug nanocarriers, the future of chemotherapy, European Journal of Pharmaceutics and Biopharmaceutics, 93 (2015) 52-79.

[43] F. Danhier, To exploit the tumor microenvironment: Since the EPR effect fails in the clinic, what is the future of nanomedicine?, Journal of Controlled Release, 244 (2016) 108-121.

[44] Y. Nakamura, A. Mochida, P.L. Choyke, H. Kobayashi, Nanodrug Delivery: Is the Enhanced Permeability and Retention Effect Sufficient for Curing Cancer?, Bioconjugate Chemistry, 27 (2016) 2225-2238.

[45] M. Overchuk, G. Zheng, Overcoming Obstacles in the Tumor Microenvironment: Recent Advancements in Nanoparticle Delivery for Cancer Theranostics, Biomaterials, (2017).

[46] M. Patra, T. Joshi, V. Pierroz, K. Ingram, M. Kaiser, S. Ferrari, B. Spingler, J. Keiser, G. Gasser, DMSO-mediated ligand dissociation: renaissance for biological activity of N-heterocyclic-[Ru(η6-arene)Cl_2] drug candidates, Chem. Eur. J., 19 (2013) 14768-14772.

[47] B. Pucelik, L.G. Arnaut, G. Stochel, J.M. Dąbrowski, Design of Pluronic-Based Formulation for Enhanced Redaporfin-Photodynamic Therapy against Pigmented Melanoma, ACS Appl. Mater. Interfaces, 8 (2016) 22039−22055.

[48] W. Zhang, Y. Shi, Y. Chen, J. Hao, X. Sha, X. Fang, The Potential of Pluronic Polymeric Micelles Encapsulated with Paclitaxel for the Treatment of Melanoma Using Subcutaneous and Pulmonary Metastatic Mice Models, Biomaterials, 32 (2011) 5934−5944.

[49] M. Zaki, F. Arjmand, S. Tabassum, Current and future potential of metallo drugs: Revisiting DNA-binding of metal containing molecules and their diverse mechanism of action, Inorganica Chimica Acta, 444 (2016) 1-22.

Polymeric micelle-mediated delivery of half-sandwich ruthenium(II) complexes with phosphanes derived from fluoroloquinolones for lung adenocarcinoma treatment

Przemysław Kołoczek[a], Agnieszka Skórska-Stania[a], Agnieszka Cierniak[b], Victor Sebastian[c,d], Urszula K. Komarnicka[e], Michał Płotek[a,f], Agnieszka Kyzioł[a*]

[a] *Faculty of Chemistry, Jagiellonian University in Krakow, Gronostajowa 2, 30-387 Krakow, Poland*

[b] *Department of General Biochemistry, Faculty of Biochemistry, Biophysics and Biotechnology, Jagiellonian University, Gronostajowa 7, 30-387 Kraków, Poland*

[c] *Department of Chemical Engineering, Aragon Institute of Nanoscience (INA), University of Zaragoza, Campus Río Ebro-Edificio I+D, Mariano Esquillor S/N, 50018 Zaragoza, Spain*

[d] *Networking Research Center on Bioengineering, Biomaterials and Nanomedicine, CIBER-BBN, 28-029 Madrid, Spain*

[e] *Faculty of Chemistry, University of Wroclaw, Joliot-Curie 14, 50-383 Wroclaw, Poland*

[f] *Faculty of Conservation and Restoration of Works of Art, Jan Matejko Academy of Fine Arts in Krakow, Lea 27-29, 30-052 Krakow, Poland*

Corresponding author e-mail address: kyziol@chemia.uj.edu.pl

Abstract

New ruthenium complexes with aminomethylphosphines derived from fluoroloquinolones (RuPCp, RuPSf, RuPLm, RuPNr)

Keywords: ruthenium(II) complexes, fluoroquinolones, polymeric micelles,

Table S1. Crystallographic experimental details.

Parameters	**RuPCp**·$CHCl_3$·$0.5CH_3CN$	**2RuPSf**·$2CHCl_3$	**RuPLm**·$2CHCl_3$	**RuPNr**·$2CHCl_3$
Moiety formula	$RuCl_5FPN_{3.5}O_3C_{42}H_{44}$	$Ru_2Cl_{10}F_4P_2N_8O_6C_{86}H_{96}$	$RuCl_8F_2PN_3O_3C_{42}H_{46}$	$RuCl_8FPN_3O_3C_{41}H_{45}$
Formula weight ($g \cdot mol^{-1}$)	974.1	2032.3	1094.5	1062.4
Crystal size (mm)	0.20 x 0.15 x 0.05	0.20 x 0.10 x 0.03	0.39 x 0.13 x 0.12	0.30 x 0.05 x 0.05
Temperature (K)	121	126	119	130
Type of radiation	Mo *Kα*	Mo *Kα*	Mo *Kα*	Mo *Kα*
Crystal system	Triclinic	Triclinic	Monoclinic	Triclinic
Space group	P $\bar{1}$	P $\bar{1}$	P $2_1/n$	P $\bar{1}$
		Unit cel dimensions		
a (Å)	12.2875(4)	13.7041(3)	29.2597(6)	11.2574(2)
b (Å)	12.3091(4)	16.8129(6)	16.9010(3)	14.6608(7)
c (Å)	14.4938(4)	20.9633(6)	9.8988(2)	15.7165(6)
α (°)	93.860(3)	71.016(3)	90	116.613(4)
β (°)	90.244(3)	75.581(2)	109.865(2)°	95.054(2)
γ (°)	105.051(3)	78.123(3)	90	95.231(3)
Volume ($Å^3$)	2111.62(12)	4382.2(2)	4603.85(17)	2285.07(16)
Z	2	2	4	2
Density calc. (g/cm^3)	1.532	1.540	1.578	1.544
Absorption coeff. (mm^{-1})	0.774	0.752	0.890	0.891
F(000)	995	2080	2220	1080
$\theta_{min} - \theta_{max}$ (°)	2.9954 to 28.550	2.841 to 28.601	2.961 to 28.699	2.930 to 28.522
hkl range	-15 ← h ← 16 -16 ← k ← 15 -19 ← l ← 18	-18 ← h ← 18 -22 ← k ← 22 -27 ← l ← 26	-39 ← h ← 38 -21 ← k ← 22 -13 ← l ← 13	-14 ← h ← 14 -18 ← k ← 19 -20 ← l ← 20
Reflections collected	30334	66135	65161	30595
Independent reflections	9763	20347	11131	10379
R_{int}	0.0340	0.0724	0.0690	0.0485
Completeness to θ_{full} (%)	99.5	99.8	99.7	99.3
Absorption correction type	Multi-scan	Semi-empirical from equivalents	Gaussian	Multi-scan
T_{max} and T_{min}	1.000 and 0.885	1.000 and 0.520	0.949 and 0.883	1.000 and 0.707
Data/restraints/parameters	9763 / 0 / 519	20347 / 0 / 1087	11131 / 0 / 558	10379 / 0 / 537
Goodness of fit F^2	1.049	1.035	1.188	1.047
R_1, wR_2 [I>2σ(I)]	0.0376, 0.0912	0.0628, 0.1429	0.0749, 0.1677	0.0671, 0.1809
R_1, wR_2 (all data)	0.0508, 0.1002	0.1129, 0.1759	0.0959, 0.1762	0.0886, 0.2006
Largest diff. peak and hole ($e Å^{-3}$)	1.134, -1.038	1.847, -1.432	1.660, -0.707	3.013, -1.694

Table S2. Comparison of ^{1}H NMR data for: starting complex **1** ({[Ru(η^6-*p*-cymene)Cl]$_2$(μ-Cl)$_2$}), phosphanes **PCp** (PPh_2**Cp**), **PSf** (PPh_2**Sf**), **PLm** (PPh_2**Lm**), **PNr** (PPh_2**Nr**) and obtained coordination compounds **RuPCp** ([Ru(η^6-*p*-cymene)(**PCp**)Cl$_2$]), **RuPSf** ([Ru(η^6-*p*-cymene)(**PSf**)Cl$_2$]), **RuPLm** ([Ru(η^6-*p*-cymene)(**PLm**)Cl$_2$]), **RuPNr** ([Ru(η^6-*p*-cymene)(**PNr**)Cl$_2$])

	DRu		**PCp** [2]		**PSf** [1]		**PLm** [3]		**PNr** [4]		**RuPCp**		**RuPSf**
Atom	**δ [ppm] (int.)**	**mult. J [Hz]**	**δ [ppm] (int.)**	**mult. J [Hz]**	**δ [ppm] (int.)**	**mult. J [Hz]**	**δ [ppm] (int.)**	**mult. J [Hz]**	**δ [ppm] (int.)**	**mult. J [Hz]**	**δ [ppm] (int.)**	**mult. J [Hz]**	**δ [ppm] (int.)**
								^{1}H NMR					
H^{1,3}	1.22 (12H)	d J = 6.9	–	–	–	–	–	–	–	–	0.88 (6H)	d J = 6.8	0.96 (6H)
H^{2}	2.87 (2H)	spt J = 7.0	–	–	–	–	–	–	–	–	2.47 (1H)	spt J = 6.9	2.48 (1H)
H^{5,9}	5.42 (4H)	d J = 5.9	–	–	–	–	–	–	–	–	5.26 (2H)	d J = 5.9	5.15 (4H)
H^{6,8}	5.29 (4H)	d J = 5.9	–	–	–	–	–	–	–	–	5.13 (2H)	d J = 5.7	
H^{10}	2.10 (6H)	s	–	–	–	–	–	–	–	–	1.84 (3H)	s	1.78 (3H)
H^{11}	–	–	3.29	d J = 2.9	3.93	bs	2.80 (2H)	bs	3.29	d J = 2.8	3.89 (2H)	s	4.05 (2H)
H^{12,15}	–	–	3.37	–	3.20	m			3.36	m	2.92 (4H)	bs	2.29 (2H)
H^{13,14}	–	–	2.90	–	3.93	m	2.95-3.45	–	2.89	m	2.28 (4H)	bs	2.76, 2.95 (2H, 2H)
H^{16}	–	–	–	–	0.94	d J = 5.9	0.97 (3H)	d J = 5.7	–	–	–	–	0.89 (3H)
H^{17}	–	–	–	–			–	–	–	–	–	–	
H^{42}	–	–	7.34-7.47	–	7.29-7.65	–	7.03-7.60 (12H)	–	7.33-7.46	–	7.97-8.13 (4H)	m	7.98-8.17 (4H)
H^{43,44}	–	–									7.41-7.62 (6H)	m	7.40-7.60 (6H)
H^{63}	–	–	7.95	d J = 13.8	6.46	bs (-NH_2)	7.84 (1H)	d J = 11.4	7.95	d J = 13.0	7.89 (1H)	d J = 13.3	6.39 (2H)
H^{67}	–	–	8.71	s	8.62	s	8.52 (1H)	S	8.63	s	8.70 (1H)	s	8.60 (1H)
H^{69}	–	–	7.34-7.47	–	–	–	–	–	6.82	d J = 6.8	7.13 (1H)	d J = 7.1	–
H^{70}	–	–	15.01	s	14.54	bs	14.65 (1H)	bs	15.13	bs	14.99 (1H)	s	14.61 (1H)
H^{71}	–	–	3.53	m	3.93	bs	4.39 (2H)	d J = 3.6	4.31	m	3.46 (1H)	bs	3.85 (1H)
H^{72}	–	–	1.18	m	1.07-1.21	m	1.48 (3H)	t J = 3.7	1.56	m	1.05-1.40 (4H)	m	1.02-1.27 (4H)
H^{73}	–	–					–	–	–	–			
								^{31}P{^{1}H} NMR					
P^{1}	–	–	-27.4	s	-35.9	s	-28.8	s	-27.5	s	27.0	s	25.7

δ – chemical shift, int. – intensity of signal, J – coupuling constant, mult. – multiplicity: s – singlet, d – doublet, t – triplet, q – quartet, spt – septet, m – multiplet, b – broad

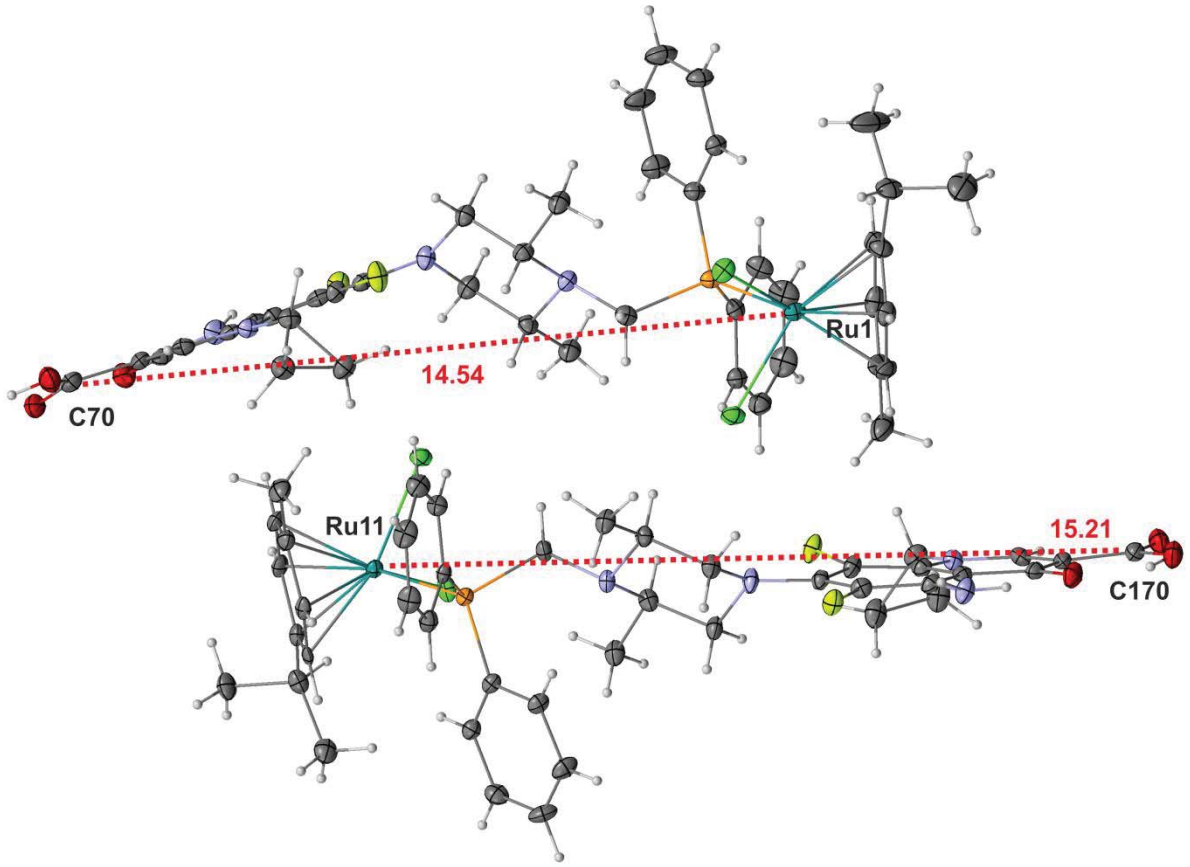

Fig. S1 Crystal structure of complex **RuPSf** with indicated Ru1-C70 distances.

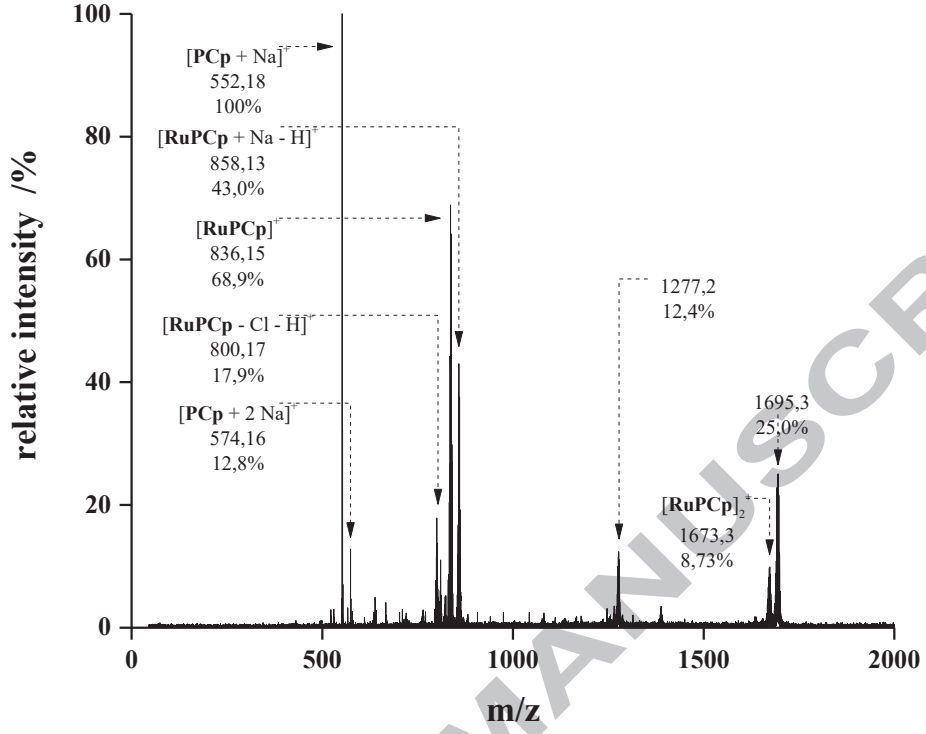

Fig. S2 +ESI mass spectrum of complex **RuPCp**.

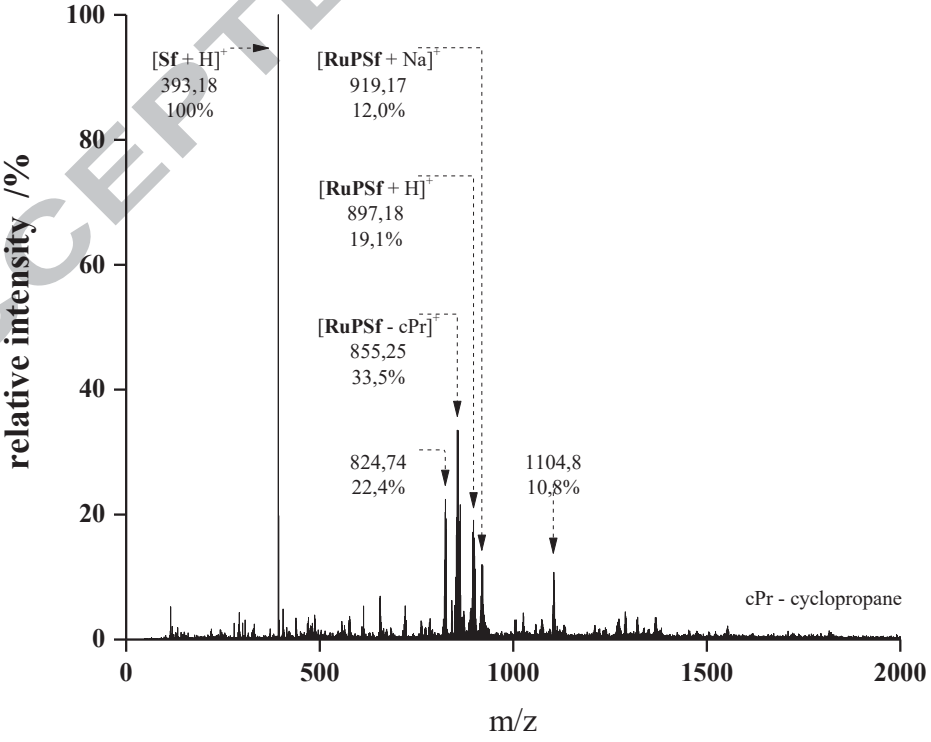

Fig. S3 +ESI mass spectrum of complex **RuPSf**.

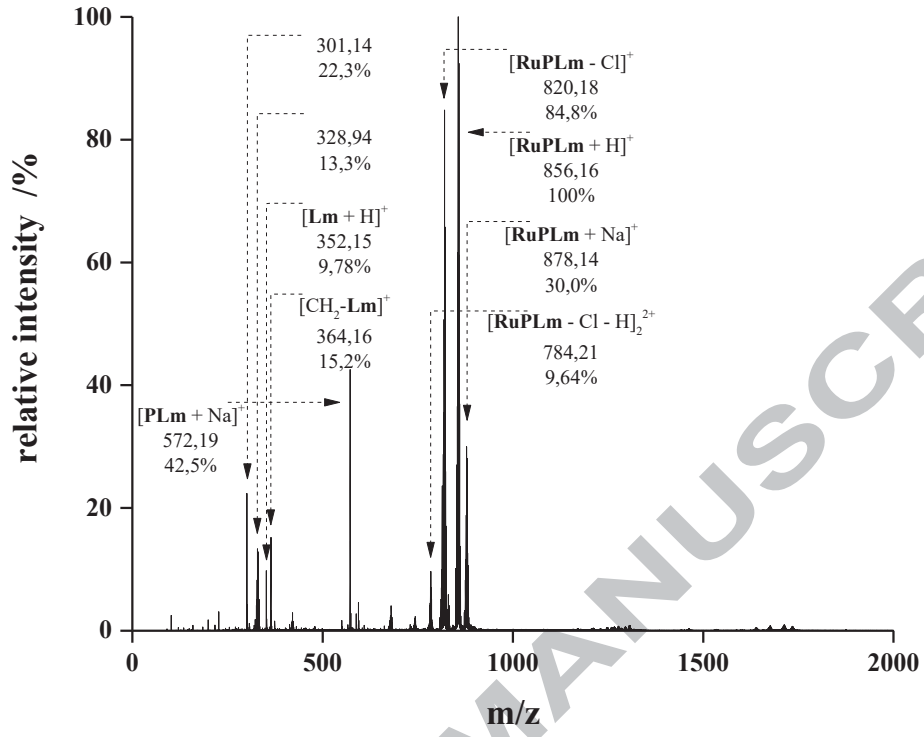

Fig. S4 +ESI mass spectrum of complex **RuPLm**.

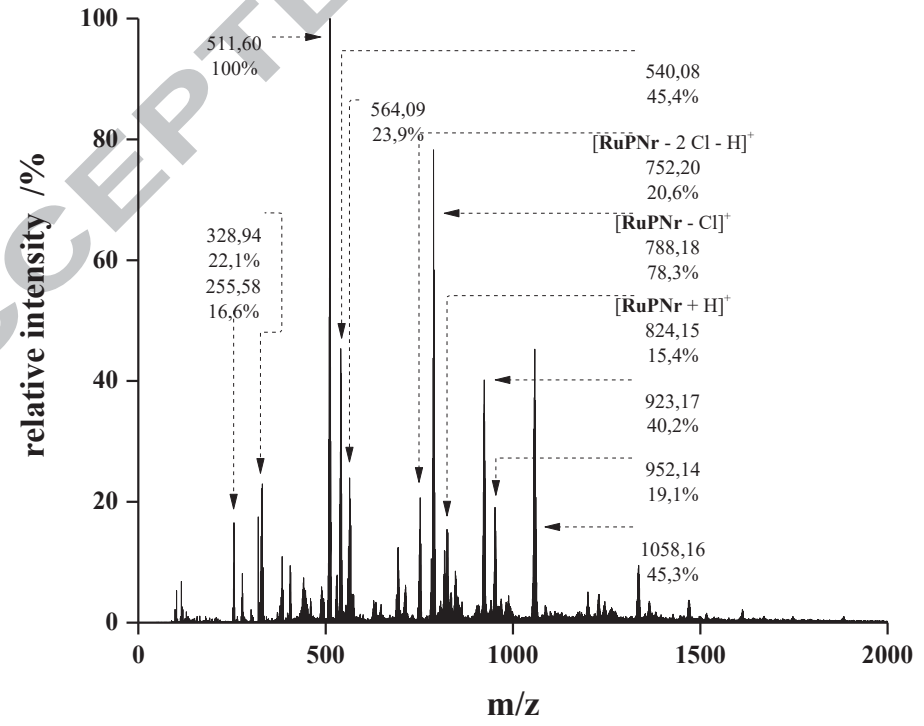

Fig. S5 +ESI mass spectrum of complex **RuPNr**.

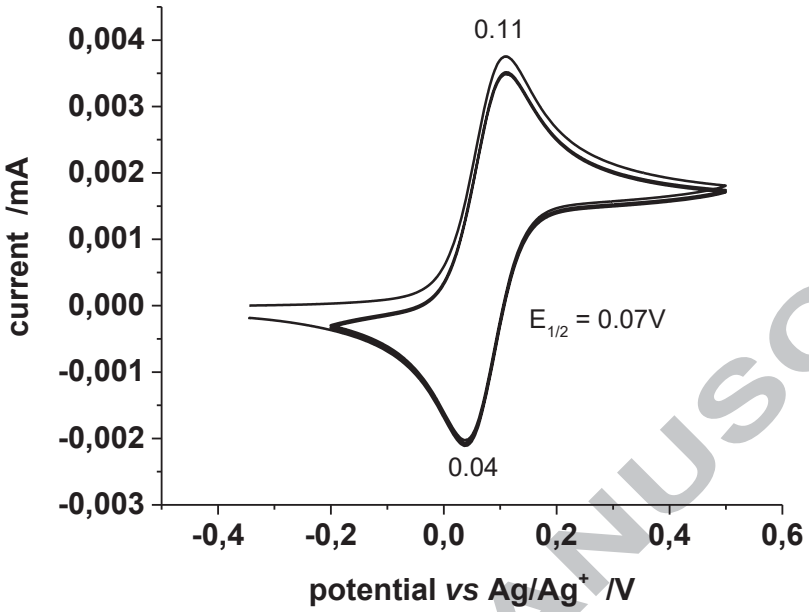

Fig. S6 CV voltammograms for ferrocene in DMF in the range of potentials from -0.2 V to 0.5 V. Scan rate: 10 mV s^{-1}.

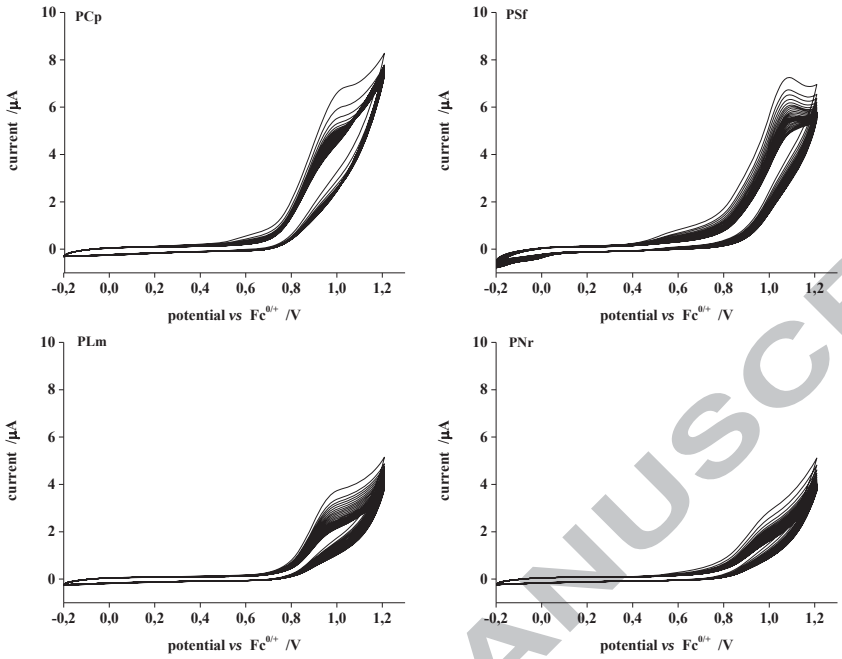

Fig. S7 Cyclic voltammograms of **PCp**, **PSpf**, **PLm**, and **PNr** in DMF (5 mM). Scan rate: 100 mV/s. The potentials were referenced to the $Fc^{0/+}$ redox couple.

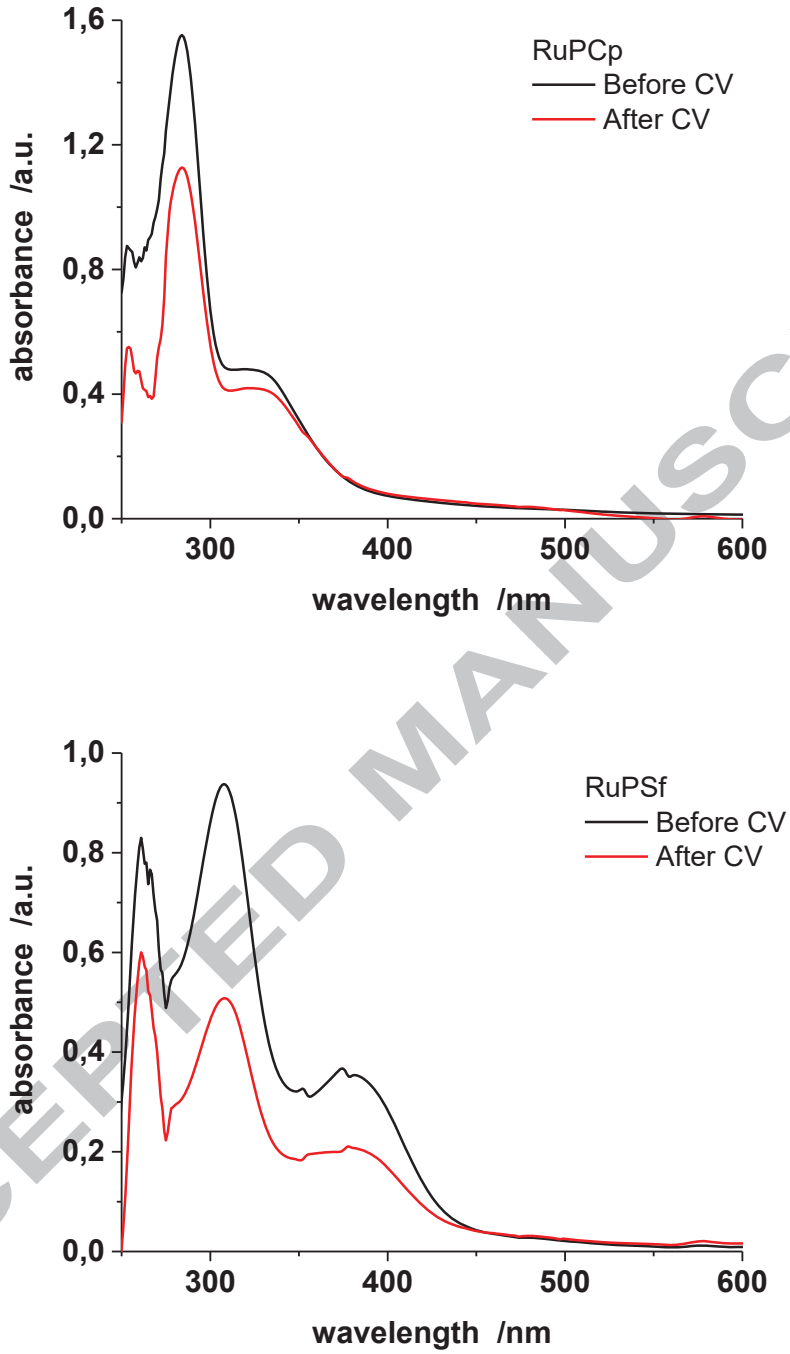

Fig. S8 Selected UV-vis spectra before and after CV experiment for **RuPCp** and **RuPSf** ruthenium(II) complexes.

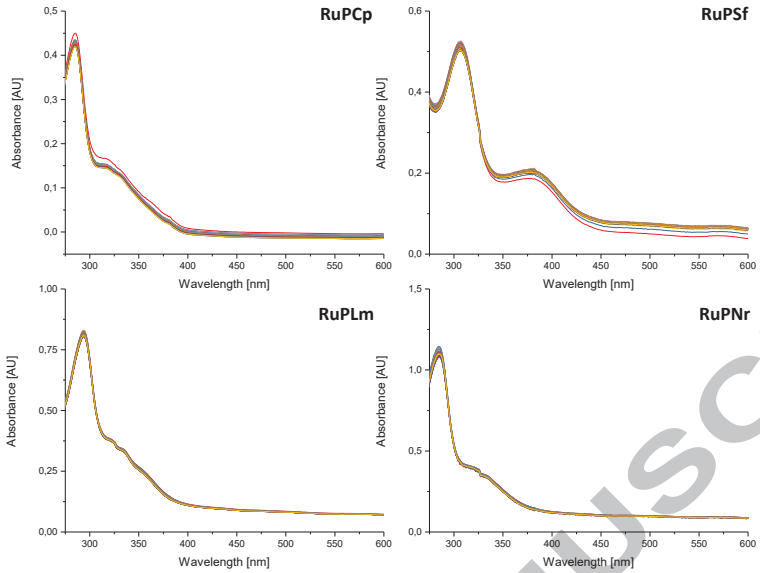

Fig. S9 UV-vis spectra of studied ruthenium(II) complexes in dimethylformamide (DMF) recorded during 24 hours at 25ºC.

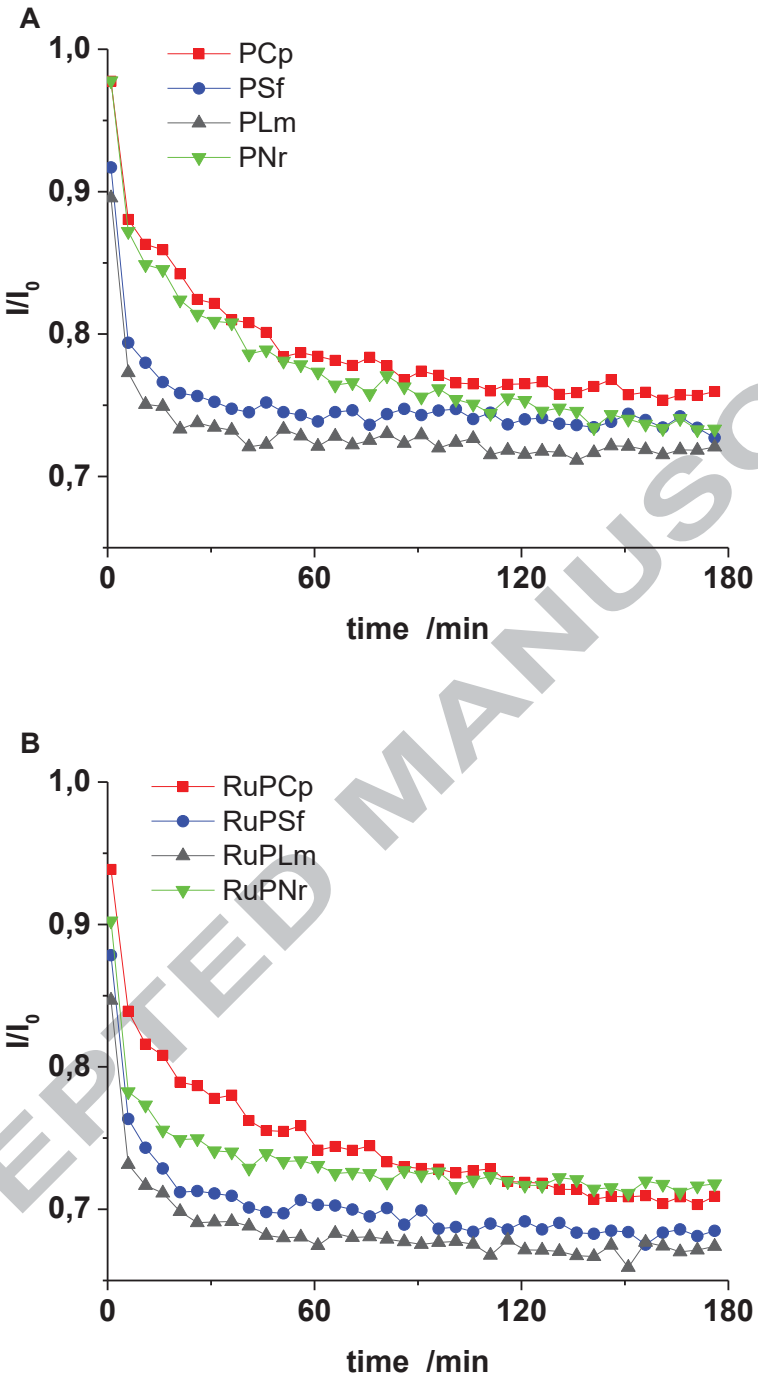

Fig. S10 Dependency of fluorescence intensities ratios on time at the emission wavelength of 605 nm, in the presence (I) and absence (I_0) of the tested ligand (**A**), and Ru(II) compounds (**B**) in a system with CT-DNA-EB.

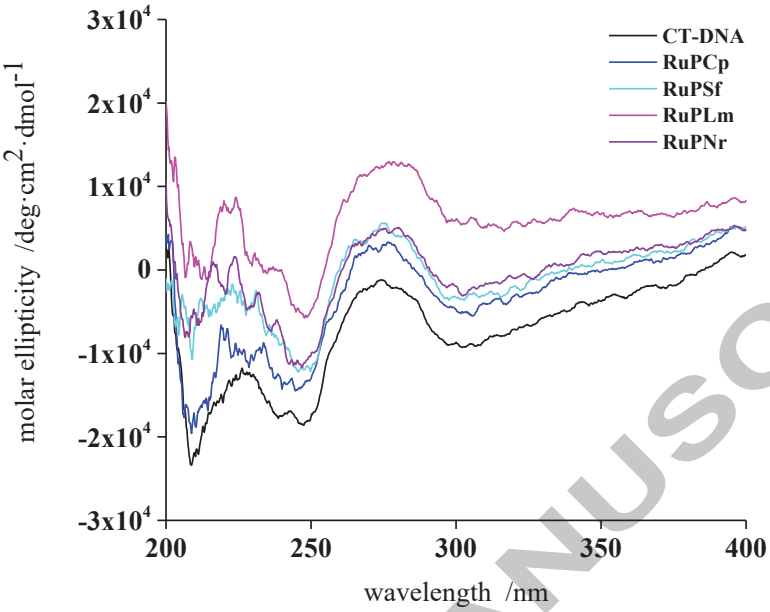

Fig. S11 Circular dichroism spectra of studied arene Ru(II) compounds in a system with CT-DNA.

HIGHLITHS

- Half-sandwich Ru(II) complexes with phosphanes derived from fluoroloquinolones are synthesized
- Half-sandwich Ru(II) complexes intercalate with DNA not causing conformation changes
- Half-sandwich Ru(II) complexes cause cleavage of a single DNA strand
- Polymeric micelles loaded with Ru(II) complexes enable efficient complex accumulation inside cancer cells
- Polymeric micelles loaded with Ru(II) complexes exhibit promising anticancer activity *in vitro*

GRAPHICAL ABSTRACT